

CONFIDENTIAL

Copy
RM L55E25

NACA RM L55E25

NOT TO BE TAKEN FROM THIS ROOM



RESEARCH MEMORANDUM

EFFECTS OF COMBINING AUXILIARY BLEED WITH EJECTOR PUMPING
ON THE POWER REQUIREMENTS AND TEST-SECTION FLOW
OF AN 8-INCH BY 8-INCH SLOTTED TUNNEL

By B. H. Little, Jr., and James M. Cabbage, Jr.

Langley Aeronautical Laboratory
Langley Field, Va.

CLASSIFICATION CHANGED

LIBRARY COPY

UNCLASSIFIED

JUL 21 1955

To
By authority of *NACA Res abs*
RN-115 Date *effective 5-8-57*
at 5-29-57

LANGLEY AERONAUTICAL LABORATORY
LIBRARY, NACA
LANGLEY FIELD, VIRGINIA

This material contains information affecting the National Defense of the United States within the meaning of the espionage laws, Title 18, U.S.C., Secs. 793 and 794, the transmission or revelation of which in any manner to an unauthorized person is prohibited by law.

NATIONAL ADVISORY COMMITTEE FOR AERONAUTICS

WASHINGTON

July 19, 1955

CONFIDENTIAL

NATIONAL ADVISORY COMMITTEE FOR AERONAUTICS

RESEARCH MEMORANDUM

EFFECTS OF COMBINING AUXILIARY BLEED WITH EJECTOR PUMPING
ON THE POWER REQUIREMENTS AND TEST-SECTION FLOW
OF AN 8-INCH BY 8-INCH SLOTTED TUNNEL

By B. H. Little, Jr., and James M. Cabbage, Jr.


SUMMARY

An investigation was made to determine the effects of combining auxiliary bleed with ejector pumping on the power requirements and test-section flow of an 8-inch by 8-inch slotted tunnel. The development of this tunnel for operation with ejection alone is described in NACA RM L55B08. The present investigation covered a Mach number range from 0.9 to 1.3 at corresponding Reynolds numbers from 11×10^6 to 18×10^6 per foot.

The effects of bleed were generally dependent upon the ejector- or slot-flow reentry-section configuration of the tunnel. The flow in the upstream part of the test section was not significantly affected by the use of auxiliary bleed, but in the downstream part of the test section, the Mach number distributions were adversely affected by auxiliary bleed with slot-flow reentry flaps 1 tunnel height in length. Reducing the flap length to about one-half the tunnel height relieved this condition.

The use of bleed reduced the diffuser-inlet Mach number and improved the diffuser-inlet boundary-layer velocity distribution so that overall tunnel pressure losses were reduced. The short-flap configuration, which was the poorer ejector configuration and required more power without bleed, benefited more by the use of bleed than did the long-flap configuration. In both configurations, however, the total power reduction was limited to the point at which the power required to handle the bleed flow equaled the power gained by reducing tunnel pressure losses.

Although, for the short flaps, minimum power was required by using minimum ejection and maximum bleed and, for the long flaps, by combining some ejection with relatively small quantities of bleed, the differences in minimum power requirements for the two configurations were negligible. The position of the slot-flow-reentry flaps was important for maximum ejector efficiency.



INTRODUCTION

For equal Mach numbers, pressure losses are considerably higher for slotted tunnels than for solid-wall tunnels. In slotted tunnels which operate on the ejector principle - using the energy of the main stream at the end of the test section to pump the slot flow into the diffuser inlet - much of the overall tunnel pressure loss may be attributed to the ejector and to the detrimental effects of this low-energy slot flow on the diffuser performance. These facts are demonstrated in reference 1 where the distribution of losses through an ejector-type tunnel is shown and in reference 2 where diffuser performance in a slotted-tunnel circuit is compared with the performance of the same diffuser with a good inlet flow produced by a contracting inlet bell. The experimental evidence indicates that it is necessary to make a careful analysis of methods of returning slot flow to the main stream before slotted-tunnel losses can be minimized.

In many cases of slotted-tunnel operation, some or all of the slot flow has been removed from the test-section plenum chamber by means of auxiliary bleed pumps. Not only does this method permit increasing the Mach number without increasing the main drive power, but also it offers the possibility of lower total-power requirements than could be obtained by using ejection alone. In reference 3 for a slotted tunnel and reference 4 for a perforated-wall tunnel, power calculations based on diffuser-exit static pressure and the settling-chamber total pressure indicate that substantial reductions in total-power requirements can be obtained by using bleed in combination with ejection. The same conclusions were reached in reference 5 for another perforated-wall tunnel. The effects of using large amounts of bleed on slotted-test-section Mach number distributions have not been pointed out in any of the available references, however, and it is not known whether the use of bleed in established slotted tunnels will affect the test-region flow.

The purpose of this investigation was to determine experimentally the effects of auxiliary bleed on test-section Mach number distributions in a slotted tunnel and to measure the power requirements of that tunnel for various combinations of bleed flow and ejector pumping. The slotted tunnel used in this investigation had an 8-inch by 8-inch test section and a 6.4° conical diffuser. Two ejector configurations were used. Local Mach numbers along the test-section center line and mean total-pressure measurements at the diffuser exit are presented for test-section Mach numbers from about 0.9 to 1.3 at corresponding Reynolds numbers from about 11×10^6 per foot to 18×10^6 per foot.

SYMBOLS

a_0	velocity of sound at reference total temperature
A^*	cross-sectional area at tunnel throat (61.2 sq in.)
C	total periphery of test section
h	height of test section at tunnel throat (8 in.)
H_0	reference total pressure
$\overline{H_e}$	mean total pressure at diffuser exit
ΔH_T	difference in total pressure from tunnel entrance cone to diffuser exit, $H_0 - \overline{H_e}$
L	length of slot-opening taper
m	mass flow
m'	bleed mass flow
M	Mach number
M_c	Mach number computed by using p_c and H_0
n	number of slots per wall
p_c	static pressure in test-section plenum chamber
T_0	reference total temperature
v	free-stream velocity
w_s	width of untapered portion of slot
δ_F	flap-position angle
ρ	free-stream density
ρ_0	density at pressure H_0 and temperature T_0

γ ratio of specific heats (1.40 for air)
 R gas constant

APPARATUS AND METHODS

The slotted tunnel used in this investigation is shown in figure 1. The development of this tunnel and its performance characteristics without auxiliary bleed were described in reference 2. The 8-inch by 8-inch test section is slotted on two opposite walls. Corner fillets reduce the cross-sectional area to 61.2 square inches at the tunnel throat. In each slotted wall are three slots, the width of the slots being such that the number of slots for a single wall n times the slot width w_s divided by one-fourth the test-section periphery C is

$$\frac{nw_s}{C/4} = \frac{1}{7}. \text{ From the tunnel throat, the slots open with a straight taper}$$

$1/2$ tunnel height in length; the slot width thereafter is maintained constant for $1\frac{1}{2}$ or 2 tunnel heights, depending upon the ejector configuration. The two ejector configurations used in this investigation were the long-flap and the short-flap configurations shown in figure 2 and described in detail in reference 2. The basic differences between these configurations were: First, the leading edge of the long flap extended forward $8\frac{3}{4}$ inches from the end of the slotted floors and the short flaps $3\frac{1}{2}$ inches from the same reference; second, since the slotted-wall plates began to taper or boattail at the flap leading edge, the boattails also were $8\frac{3}{4}$ and $3\frac{1}{2}$ inches long, respectively; and third, the slot lengths were also varied by the same amounts since the start of the boattail determined the end of the constant-width slot. The flaps were hinged at the trailing edge so that the flap leading edge and angle relative to the flow controlled the ejector pumping. The flap positions used for these tests are indicated in figure 2. The flap-position angle was measured from the most closed position of the flap which, for the long flaps, was determined when the leading edge made contact with the slotted-wall plates and for the short flaps when the leading edge made contact with the corner-fillet inserts.

Since the slot-flow reentry flaps were outboard of the slotted walls, the cross-sectional shape at the end of the test section was rectangular rather than square with an area 1.16 times the tunnel-throat area. The transition section faired into the flap upper surface and, in a length of

about 11 inches, performed the geometric conversion to a circle at the diffuser inlet. The area increased slightly through the transition section to 1.19 times the tunnel-throat area at the diffuser inlet.

The diffuser had an included conical angle of 6.4° and a ratio of exit area to inlet area of 2.4. The elbow following the diffuser was designed to simulate the first corner of a closed-circuit tunnel. All of the tunnel components are described in more detail in reference 2.

The flow circuit through the tunnel is shown in figure 3. Air was supplied by multistage centrifugal compressors capable of delivering a maximum air flow of 60 lb/sec at pressures up to 50 lb/sq in. abs. The stagnation temperature was variable but was generally set at about 150° F or whatever higher value was necessary to avoid visible condensation in the test section. The circuit was of the nonreturn type exhausting to atmosphere, but a butterfly valve in the exhaust ducting controlled the back pressure of the diffuser. Since no auxiliary pumps were available, it was necessary that the diffuser back pressure be high enough to maintain the test section at a pressure greater than atmospheric pressure in order that air could be bled from the test section. The auxiliary bleed flow passed from the test-section plenum chambers, outboard of the slotted walls, into the bleed manifolds. From the manifolds, approach pipes led to venturi meters by which the flow was measured. Downstream of the venturi meters were butterfly valves which controlled the bleed flow. These bleed systems - manifolds, approach pipes, venturi meters, and butterfly valves - were calibrated as complete assemblies.

A static-pressure survey tube (shown in fig. 1) was used to obtain static-pressure distributions along the center line through the test section. This tube extended through the diffuser and tunnel elbow and was driven by a friction drive mounted outside the elbow. For some of the surveys, the static pressure was read on a U-tube manometer at each survey-tube position. Later, this system was modified so that continuous measurements of static pressure and position were recorded simultaneously on a two-variable recorder.

The reference Mach number M_c was computed from the static pressure in the slot-flow plenum chambers p_c and the reference total pressure H_0 . It was shown in reference 2 that this Mach number is a good indication of the average test-section Mach number.

Total-pressure surveys were made at the inlet and exit stations of the diffuser by using rakes mounted from the elbow which could be rotated through 360° . The exit-station rake is shown in figure 1 and the inlet-station rake is of similar construction. These rakes were connected to

multitube manometer boards. Pressure surveys were made across eight diameters $22\frac{1}{2}$ apart for each test point. These measurements were then mass-weighted as described in reference 2 to obtain the mean total pressure.

Some of the data are presented in the form of total-horsepower measurements. The total horsepower is defined as the sum of the power required to compress isentropically the slot-flow air from the pressure p_c to the reference stagnation pressure H_o and the power required to compress the main-stream air from the pressure $\overline{H_e}$ measured at the diffuser exit to H_o ; that is,

$$HP_{tot} = \frac{m'RT_o}{550} \frac{\gamma}{\gamma - 1} \left[\left(\frac{H_o}{p_c} \right)^{\frac{\gamma-1}{\gamma}} - 1 \right] + \frac{(m - m')RT_o}{550} \frac{\gamma}{\gamma - 1} \left[\left(\frac{H_o}{\overline{H_e}} \right)^{\frac{\gamma-1}{\gamma}} - 1 \right]$$

To obtain a standard horsepower term this expression was actually used in the form:

$$\frac{HP_{tot}}{A \cdot H_o \sqrt{T_o}} = \frac{\sqrt{\gamma R}}{550} \frac{\gamma}{\gamma - 1} \left(\frac{\rho v}{\rho_o a_o} \right)_{M=1.0} \left\{ \frac{\gamma - 1}{2} \frac{m'}{m} M_c^2 + \left(1 - \frac{m'}{m} \right) \left[\left(\frac{H_o}{\overline{H_e}} \right)^{\frac{\gamma-1}{\gamma}} - 1 \right] \right\}$$

In using this relationship the bleed air is assumed to be at rest at pressure p_c and any kinetic energy it possesses is neglected. The duct losses involved in returning bleed and mainstream air to the tunnel settling chamber have also been neglected.

RESULTS AND DISCUSSION

The effects of auxiliary bleed on test-section Mach number M_c .
The effects of auxiliary bleed on test-section Mach number M_c are shown in figures 4(a) and 4(b). The curves of figure 4(a) represent the basic experimental data obtained by holding total pressure constant and starting to bleed at three different M_c values (at each flap position) which were set by adjusting the tunnel back-pressure valve. As bleed was increased and M_c increased, the tunnel pressure losses also increased and the mean total pressure at the diffuser exit $\overline{H_e}$ decreased. Thus the curves of figure 4(a) represent lines along which the tunnel pressure ratio $H_o/\overline{H_e}$ increased with increasing bleed. The changes in M_c with bleed would not

be so great as shown in figure 4(a) for wind tunnels in which the ratio H_0/\overline{H}_e must be held constant. To demonstrate this, the basic-data curves of figure 4(a) have been adjusted by using the total-pressure-loss measurements to calculate the variation of M_c with m'/m at constant values of H_0/\overline{H}_e . These adjusted curves are plotted in figure 4(b).

If an initial Mach number of 1.0 is assumed, an expression for subsequent Mach numbers, as air is bled from the test section, can readily be derived from one-dimensional theory as:

$$\frac{M_c}{\left(1 + \frac{\gamma - 1}{2} M_c^2\right)^{\frac{1}{2}}} = \left(\frac{\rho v}{\rho_0 a_0}\right)_{M=1.0} \left(1 - \frac{m'}{m}\right)$$

The curve representing this relation is also shown in figure 4(b) in the plot for $\delta_F = 0^\circ$. The theoretical curve has a high rate of increase of M_c with m'/m near $M_c = 1.0$ with a gradually decreasing slope at higher Mach numbers. The experimental curves of figure 4(b) have the same general shape, but, because in practice the boundary layer through the test section must be removed, the increase in M_c with m'/m is not so great as the theory predicts. There is no significant variation in curve shape between long and short flaps or between flap positions in either configuration.

Effect of auxiliary bleed on test-section Mach number distributions.—Mach number distributions along the tunnel center line for the long- and short-flap configurations at flap angles δ_F of 0° , 5° , and 10° are presented in figures 5 and 6, and a comparison of long and short flaps at $\delta_F = 10^\circ$ with bleed is shown in figure 7. In addition to the value of M_c labeled for each distribution, the values of bleed flow rates m'/m at which the distributions were obtained are also shown. The bleed flow rate indicated for a particular value of M_c represents the maximum amount obtained for that value of M_c . It is felt, therefore, that this condition reveals the greatest effect of bleed flow upon the Mach number distributions that would ordinarily be encountered. For ease of comparison of the present data with data from reference 2, the Mach number distributions from that reference, for the identical slot and flap configurations without bleed flow, have been superimposed on the distributions of figures 5 and 6. Plan views of the slot are shown in figures 5, 6, and 7 to facilitate orientation of the distributions with respect to the

slot. The distributions of figure 6 were obtained by use of the two-variable continuous-recording potentiometer. The data points of figure 5, which were obtained by use of the U-tube manometer, have been omitted in figure 7 to clarify the comparisons between configurations.

The faster response of the recording potentiometer revealed smaller variations than could be picked up by the manometer system, and the continuous trace revealed peaks in the curves that were missed in the point selection of the manually read data. Therefore, the automatically recorded distributions appear to be somewhat more irregular than those that were manually read. While neither configuration produced test-region flows of the high quality desired for model testing, the distributions could be improved by modifying the slots in the opening-taper region (as was done in ref. 6) so that the flows would be satisfactory. It was not considered necessary that such refinements be made for these tests since the objective was to determine the major effects of bleed on the test-section flow.

In the long-flap configuration for $\delta_F = 0^\circ$ (fig. 5(a)) the use of bleed instead of ejection had no effect on the Mach number distributions except on the downstream part of the flaps. The effects in this region had little, if any, influence on the test-region flow. The distributions for $\delta_F = 5^\circ$ and 10° (figs. 5(b) and (c)), however, which were the best flap positions for the no-bleed case, were considerably affected where bleed was used. It can be seen in both figure 5(b) and 5(c) that at all supersonic Mach numbers the flow choked at a point about $1\frac{3}{4}$ inches downstream of the flap leading edge. At the higher Mach numbers ($M_c > 1.20$) the deceleration preceding this choke point started as far as 3 inches upstream of the flaps with the result that the region of uniform flow was considerably shortened.

Inspection of figure 6 shows that auxiliary bleed flow had no significant effect on the uniformity of the test-section flow or the usable test-section length for the short-flap configuration over the Mach number range investigated. The initial rate of expansion of the flow and the amount of its overexpansion is slightly greater for the no-bleed case than for the bleed case.

The long- and short-flap configurations with auxiliary bleed flow are compared in figure 7 at $\delta_F = 10^\circ$. Although, as previously mentioned, neither configuration produced entirely satisfactory test-region flow, the data show the short flaps to be superior to the long flaps for all values of $M_c > 1.0$ mainly because of choking of the tunnel with the long-flap configuration.

Effects of bleed on diffuser-inlet flow.- Some pressure distributions were measured at the diffuser-inlet cross section from which Mach number contours were computed. In figure 8, for both the long- and short-flap configurations, contours are shown for a test-section Mach number M_c of 1.15 obtained at three different rates of bleed. Going from practically no bleed ($\frac{m'}{m} = 0.003$) to about 3-percent bleed ($\frac{m'}{m} = 0.03$), the main effect is seen to be that the maximum Mach number is reduced. It can be seen in reference 2 that for Mach numbers around 1.0, a small reduction in the mean inlet Mach number of the diffuser reduces the total-pressure losses considerably. Bleed also improves diffuser performance as a result of removing the low-energy boundary-layer air behind the slots, but it is impossible from the data available to judge the amount that this contributes to the overall effect.

Effects of bleed on tunnel total-pressure loss.- The effects of bleed on the tunnel total-pressure-loss ratio $\Delta H_T/H_0$ are shown for the long flaps in figure 9 and for the short flaps in figure 10. From figure 4, lines of constant bleed rate (dashed lines) have been plotted in these figures. The zero-bleed-flow lines were obtained from reference 2. The solid lines represent the actual experimental curves which show the effect of $\Delta H_T/H_0$ increasing, and, therefore, $H_0/\sqrt{H_e}$ increasing, as m'/m is increased. In examining the curves of figures 9 and 10, it should be pointed out that these curves show only the tunnel pressure losses and give no indication of the power required to operate the bleed system. All the parts of figures 9 and 10 show generally the same type of curves. The use of bleed always shifts the performance curves in a favorable direction. The amount that the curves are shifted varies with flap position and configuration, but comparisons can more easily be made in cross plots of these figures.

In figures 11(a) and (b) for the long and short flaps, respectively, the data of figures 9 and 10 are replotted to show the variation of $\Delta H_T/H_0$ with m'/m at constant Mach numbers. Zero-bleed points could not be obtained for some of the curves (for example, $\delta_F = 0^\circ$ at $M_c = 1.2$, and $\delta_F = 0^\circ$ and 5° at $M_c = 1.3$ in figure 11(a)) because the tunnel choked at those Mach numbers unless bleed was used. Proper evaluation of the various configurations relative to each other can readily be made in these figures because for any particular combination of M_c and m'/m the power required for bleed is constant.

For the long-flap configuration (fig. 11(a)), it can be seen that $\Delta H_T/H_0$ decreases continuously as m'/m increases. The rate of decrease in $\Delta H_T/H_0$, however, is greatest at small values of m'/m and large values of M_c and the rate diminishes as M_c decreases and as m'/m

increases. The exception to this is that for cases where bleed is alleviating a choked condition large reductions in $\Delta H_T/H_0$ are always obtained with bleed as, for example, is the case for $M_c = 1.3$, $\delta_F = 0^\circ$. At M_c values up to and including 1.2 the flap position $\delta_F = 5^\circ$ gives substantially better performance than the other flap positions at all values of m'/m , and it was shown in reference 3 that for zero bleed $\delta_F = 5^\circ$ was the best position at these Mach numbers. This $\delta_F = 5^\circ$ configuration begins to choke at about $M_c > 1.2$, however, and at low values of m'/m a value for $M_c = 1.3$ cannot be reached; therefore, the flap position $\delta_F = 10^\circ$ is best at values of $m'/m < 0.04$ and $\delta_F = 5^\circ$ is best at $m'/m > 0.04$. At all Mach numbers shown in figure 11(a), the curve for $\delta_F = 0^\circ$ starts at a high value of $\Delta H_T/H_0$ at the low rates of bleed but, with increasing bleed, crosses over the curves for other flap positions, so that it appears possible that at bleed rates greater than those obtained in these tests the best flap position might be $\delta_F = 0^\circ$.

For the short-flap configuration (fig. 11(b)) the variation of $\Delta H_T/H_0$ with m'/m is similar to that for the long-flap configuration. At $M_c = 1.30$, however, all flap positions are choked without some bleed flow. There is less variation of performance with flap position than occurred for the long-flap configuration but the general results are the same. The curve for $\delta_F = 0^\circ$, however, does completely cross over the other curves so that $\delta_F = 0^\circ$ is the best flap position at the higher bleed rates measured.

Envelope curves from figures 11(a) and 11(b) are plotted in figure 12 to compare the best curves of long- and short-flap configurations when flap position is variable. Without bleed ($\frac{m'}{m} = 0$) the long flap forms the better ejector and therefore $\Delta H_T/H_0$ is lower. At low Mach numbers, the short-flap-configuration performance equals and surpasses that of the long-flap configuration as bleed is started. As M_c increases, more and more bleed is required to reach this crossover where the short flap becomes the better configuration. At $M_c = 1.3$ this point was not reached within the scope of these tests but the curves are gradually converging at the highest bleed flow rates measured.

It can be seen in figure 12 that at low Mach numbers ($M_c \leq 1.1$) with a small amount of bleed the configuration with less ejector pumping (short flaps) performs as well as the configuration with more ejector pumping. Above $M_c = 1.1$, however, increasingly larger amounts of bleed

are required for good performance without a good ejector. At $M_c = 1.3$, the differences between total-pressure loss with and without ejector pumping are considerable unless it is possible to bleed more than 5 percent of the mainstream flow.

Effects of flap position on bleed requirements.- The effect of flap position on bleed requirements is shown in figure 13(a) for the long flaps and in figure 13(b) for the short flaps. The curves plotted show for a constant M_c the amount of bleed required as δ_F changes when the ratio of stagnation total pressure to diffuser-exit total pressure is constant. The effects of flap position are quite pronounced for the long flaps. For every Mach number and pressure ratio, there is a well-defined optimum value of δ_F where minimum bleed is required. When δ_F is less than this optimum value, the flaps are not open enough to take advantage of the pumping that the ejector is able to furnish, and when δ_F is greater than this optimum value, there is a strong possibility that air is flowing from the diffuser inlet back over the flaps into the test-section plenum chamber. This back flow would be more likely to occur at low total-pressure ratios where the pressures at the diffuser inlet are high relative to the total pressure H_0 and to the plenum-chamber pressure p_c , and it can be seen in figure 13(a) that the increase in m'/m with δ_F , when δ_F is greater than the optimum value, is much more pronounced at the lower total-pressure ratios. The reason for the peak in these curves at about $\delta_F = 15^\circ$ and the decrease in m'/m with increasing δ_F thereafter is not clearly understood but the same trends were observed in reference 3. In general, the optimum value of δ_F increases with increasing $H_0/\sqrt{H_e}$ and decreasing m'/m . This is most evident at $M_c = 1.30$ but the same trend exists at the other Mach numbers.

The effects of the short flaps on bleed requirements (fig. 13(b)) are similar to but not so great as for the long flaps. There are the same increases in m'/m with increasing δ_F beyond the optimum that indicate less ejector pumping and there is also the same trend that was observed with the long flaps for the optimum flap angle to increase with decreasing m'/m . There is not nearly so much difference between best and worst short-flap position as for the long-flap position because the short-flap configuration does not function nearly so well as an ejector.

Total horsepower with auxiliary bleed.- In figure 14, envelope curves of the total air horsepower factor $\frac{HP_{tot}}{A \cdot H_0 \sqrt{T_0}}$ are plotted against m'/m for the long and short flaps at different Mach numbers. These curves represent the same data presented in figure 12. Significant reductions

in total horsepower with bleed were experienced by both long- and short-flap configurations, and since the short-flap configuration was not so efficient without bleed as the long-flap configuration, greater gains were obtained with the short flaps. However, the minimum total horsepower for the optimum amount of bleed flow is about the same for both configurations with the long flaps slightly better at the highest Mach numbers. The increase in horsepower with increasing bleed beyond a certain amount can probably be attributed to the fact that the diffuser efficiency is no longer improving and the kinetic energy of the bleed air has been neglected in the power equation.

In figure 15, total-horsepower factor is plotted against M_c for the different flap positions of both long- and short-flap configurations. The different curves at each flap position represent different values of total-pressure ratio H_0/\overline{H}_e . It can be seen that for every ejector configuration tested a higher Mach number could be reached with less power by using bleed than by raising the mainstream power (represented by the solid line). The crossing over of the bleed curves for the long flaps probably occurs when the kinetic energy of the bleed flow which is neglected in the power equation outweighs the increasing diffuser efficiency. For the short flaps, the curves with bleed tend to converge to almost a single line regardless of where bleed is started, and for best overall results bleed should probably be started at the lowest value of H_0/\overline{H}_e shown. The problem of where to start bleed is not too important as long as enough bleed is used at the design Mach number for operation on the steep-slope portion of the curves, or line of convergence; for example, if it is desired to operate at $M_c = 1.2$ with the short flaps at $\delta_F = 5^\circ$, it is not too important whether bleed is started at $H_0/\overline{H}_e = 1.09$ or 1.12 but it is important that bleed be started at $H_0/\overline{H}_e = 1.12$ rather than 1.16 or a higher value.

In figure 16, $\frac{HP_{tot}}{A^*H_0/\overline{T}_0}$ is plotted against M_c for the best operating conditions of the long and short flaps. For the long flaps, an envelope curve for $\delta_F = 5^\circ$ was chosen and for the short flaps an envelope curve for $\delta_F = 0^\circ$ was used, with both curves starting at $H_0/\overline{H}_e = 1.09$. These choices were based on the results shown in figures 11(a) and 11(b). The most obvious result is that for the best operating conditions in either configuration there is little difference in power required. It should be borne in mind, however, that these optimum-condition curves are basically different in nature, for in the long-flap configuration which functions well as an ejector, the optimum was reached with some ejector pumping and moderate amounts of bleed $\left(\frac{m'}{m} < 0.04\right)$,

whereas in the short-flap configuration which is not a good ejector the optimum was reached by using minimum ejector pumping and large amounts of bleed.

CONCLUSIONS

An investigation of the effects of slot-flow removal by means of auxiliary pumping or bleed on the test-section flow and power characteristics of an 8-inch by 8-inch slotted tunnel has led to the following conclusions:

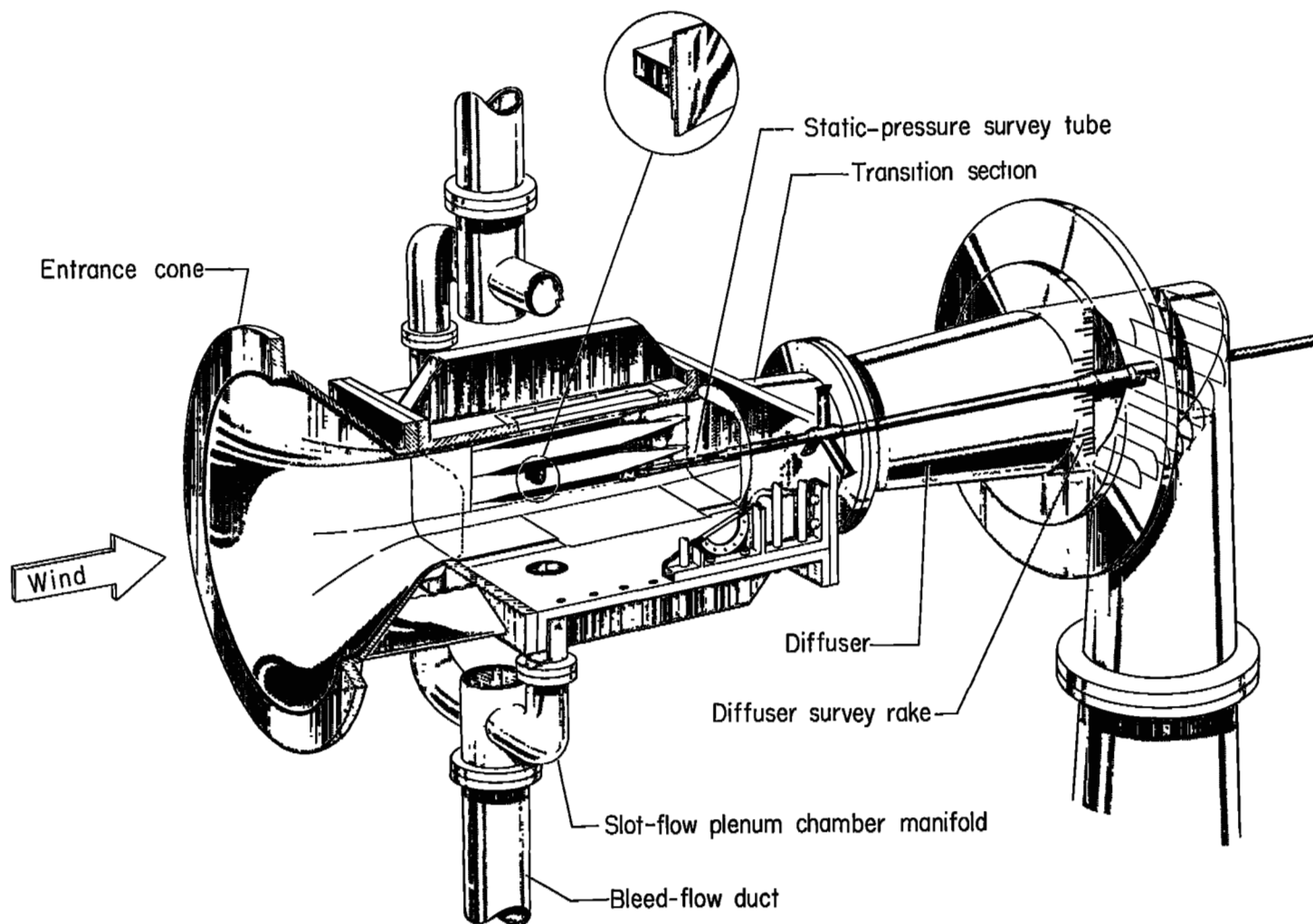
1. The region of supersonic-flow deceleration at the end of the slots was extended forward when bleed was used with slot-flow reentry flaps which were about 1 tunnel height in length; this extension reduced the available test region length considerably at the higher Mach numbers. Reducing the flap length to about 1/2 tunnel height relieved this condition. No other significant effects of bleed on the center-line Mach number distribution were observed.
2. The use of auxiliary bleed reduced the diffuser-inlet Mach number and improved the inlet boundary-layer velocity distributions. These effects combined to reduce diffuser and thereby overall tunnel pressure losses.
3. Total-power requirements decreased with increasing bleed flow to the point where the power required to handle the bleed flow was equal to the power saved through improved diffuser performance. The quantity of bleed required to reach the minimum-power point was dependent upon Mach number and ejector configuration, but the minimum-power point was always reached with a bleed flow less than 6 percent of the mainstream mass flow.
4. The reduction of tunnel pressure loss with bleed depended primarily upon the ejector characteristics of the tunnel which were affected by flap configuration and flap position. The short-flap configuration, which was the poorer ejector, gained considerably more in performance from the use of bleed than did the long-flap configuration.

5. Although, for the short flaps, minimum total power was required by using minimum ejector pumping and maximum bleed and, for the long flaps, by combining some ejector pumping with relatively small quantities of bleed, the differences in minimum total-power requirements for the two configurations were negligible.

Langley Aeronautical Laboratory,
National Advisory Committee for Aeronautics,
Langley Field, Va., May 6, 1955.

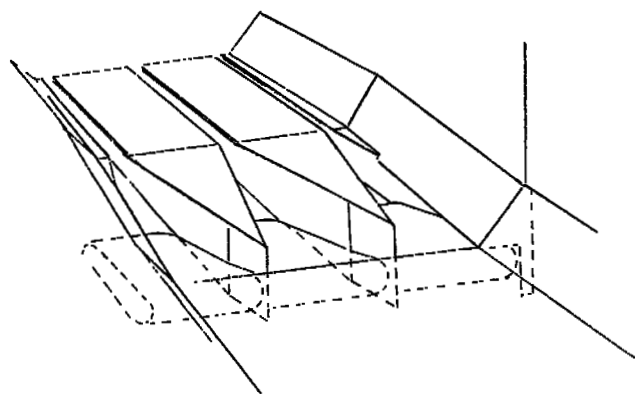
REFERENCES

1. Whitcomb, Richard T., Carmel, Melvin M., and Morgan, Francis G., Jr.: An Investigation of the Stream-Tube Power Losses and an Improvement of the Diffuser-Entrance Nose in the Langley 8-Foot Transonic Tunnel. NACA RM L52E20, 1952.
2. Little, B. H., Jr., and Cabbage, James M., Jr.: The Development of an 8-Inch by 8-Inch Slotted Tunnel for Mach Numbers up to 1.28. NACA RM L55B08, 1955.
3. Dennard, John S., and Little, Barney H., Jr.: Effects of Auxiliary and Ejector Pumping on the Mach Number Attainable in a $4\frac{1}{2}$ - by $4\frac{1}{2}$ - Inch Slotted Tunnel at Low Pressure Ratios. NACA RM L53K19, 1954.
4. Breed, Elizabeth C.: Tests of Diffuser Flaps in a Perforated Wall Transonic Wind Tunnel. Rep. M-95630-12, United Aircraft Corp. Res. Dept., Dec. 9, 1953.
5. Chew, William L.: Wind Tunnel Investigations of Transonic Test Sections. Phase I - Tests of a 22.5-Percent Open-Area Perforated-Wall Test Section in Conjunction With a Sonic Nozzle. AEDC-TR-53-10, Arnold Eng. Dev. Center, U. S. Air Force, Oct. 1953.
6. Ward, Vernon G., Whitcomb, Charles F., and Pearson, Merwin D.: Air-Flow and Power Characteristics of the Langley 16-Foot Transonic Tunnel With Slotted Test Section. NACA RM L52E01, 1952.

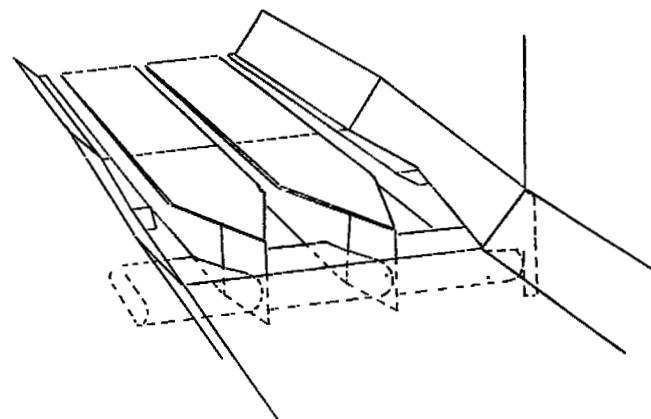


L-87573.1

Figure 1.- The 8-inch by 8-inch slotted tunnel configuration.



LONG-FLAP CONFIGURATION



SHORT-FLAP CONFIGURATION

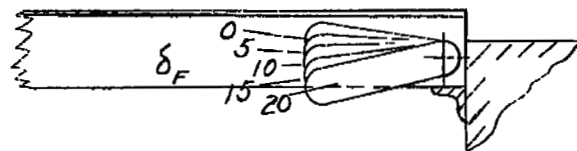
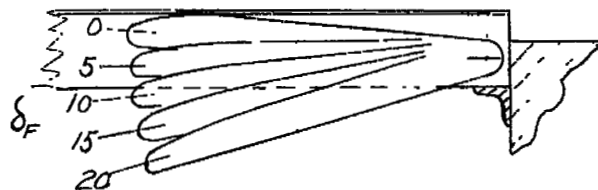


Figure 2.- Slot-flow reentry-section configurations.

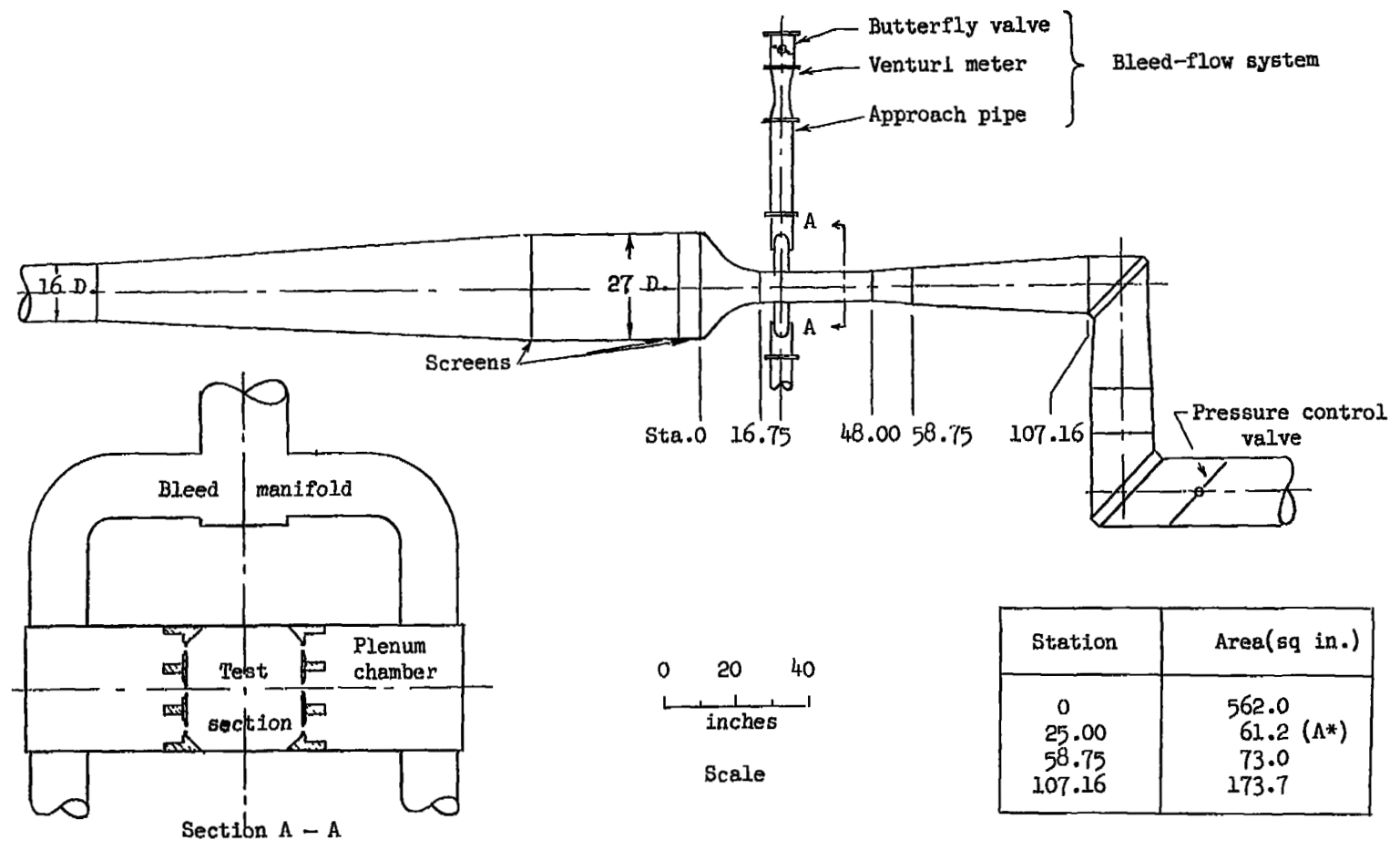
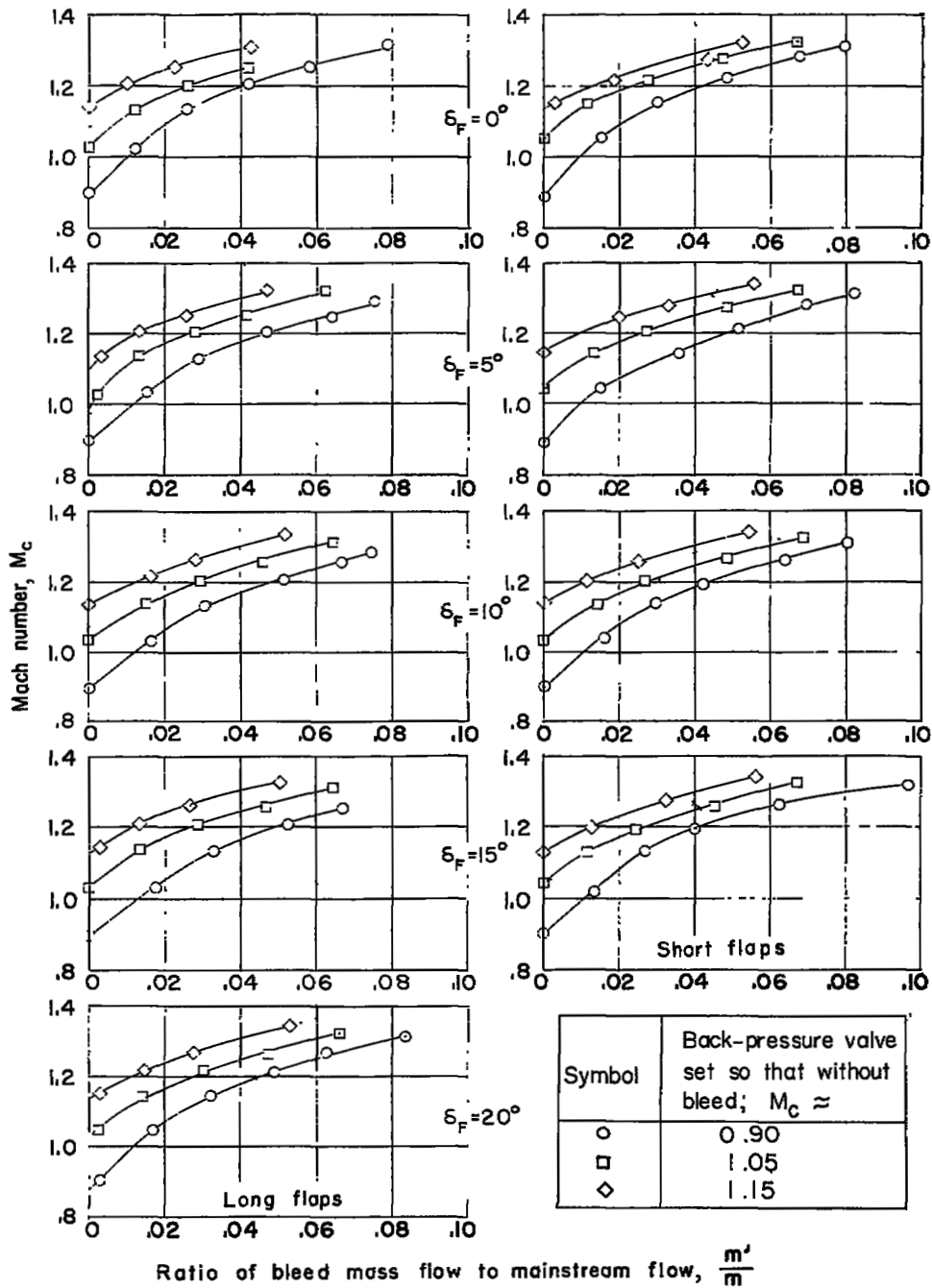
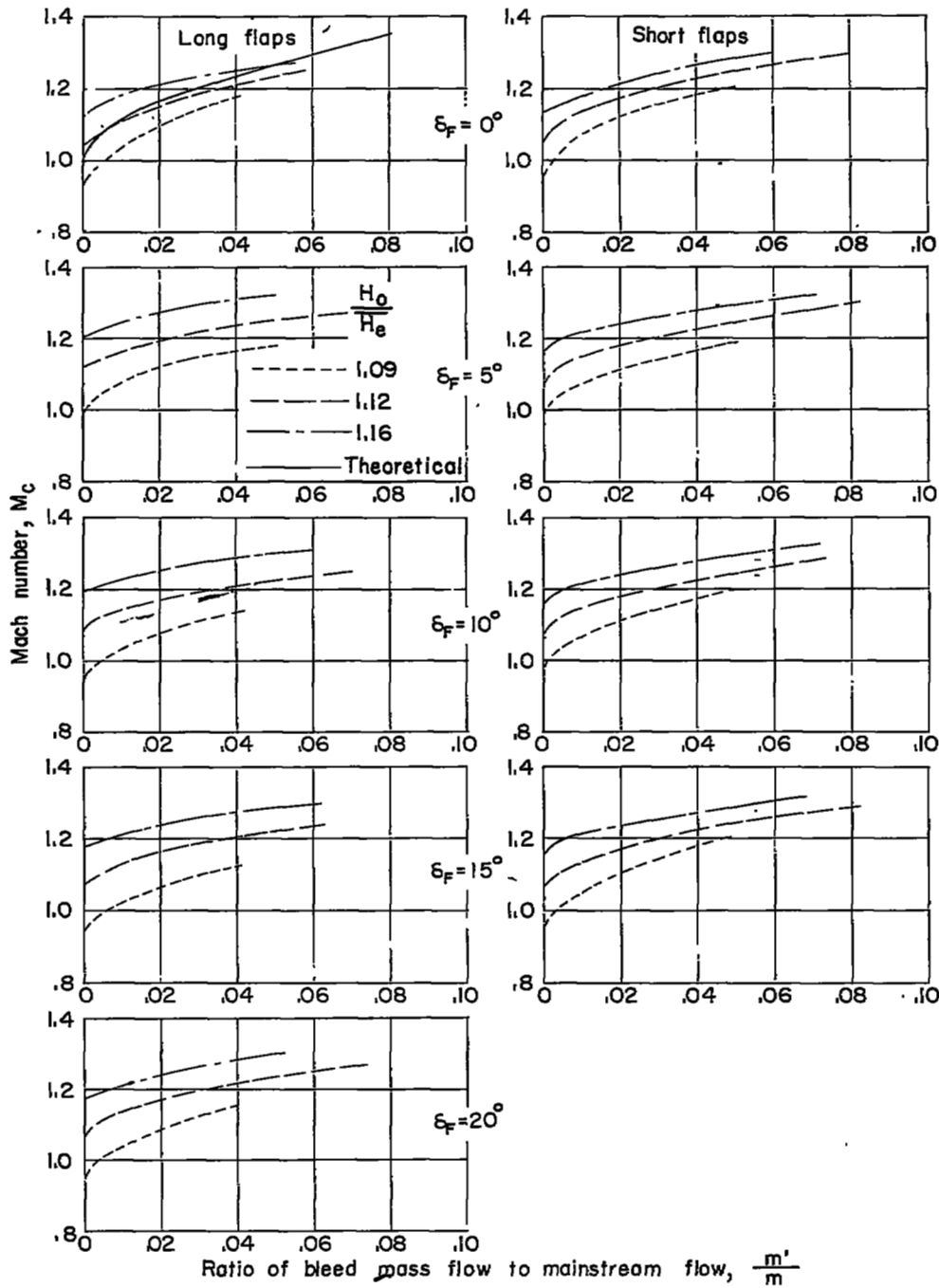


Figure 3.- Line diagram of tunnel flow system.



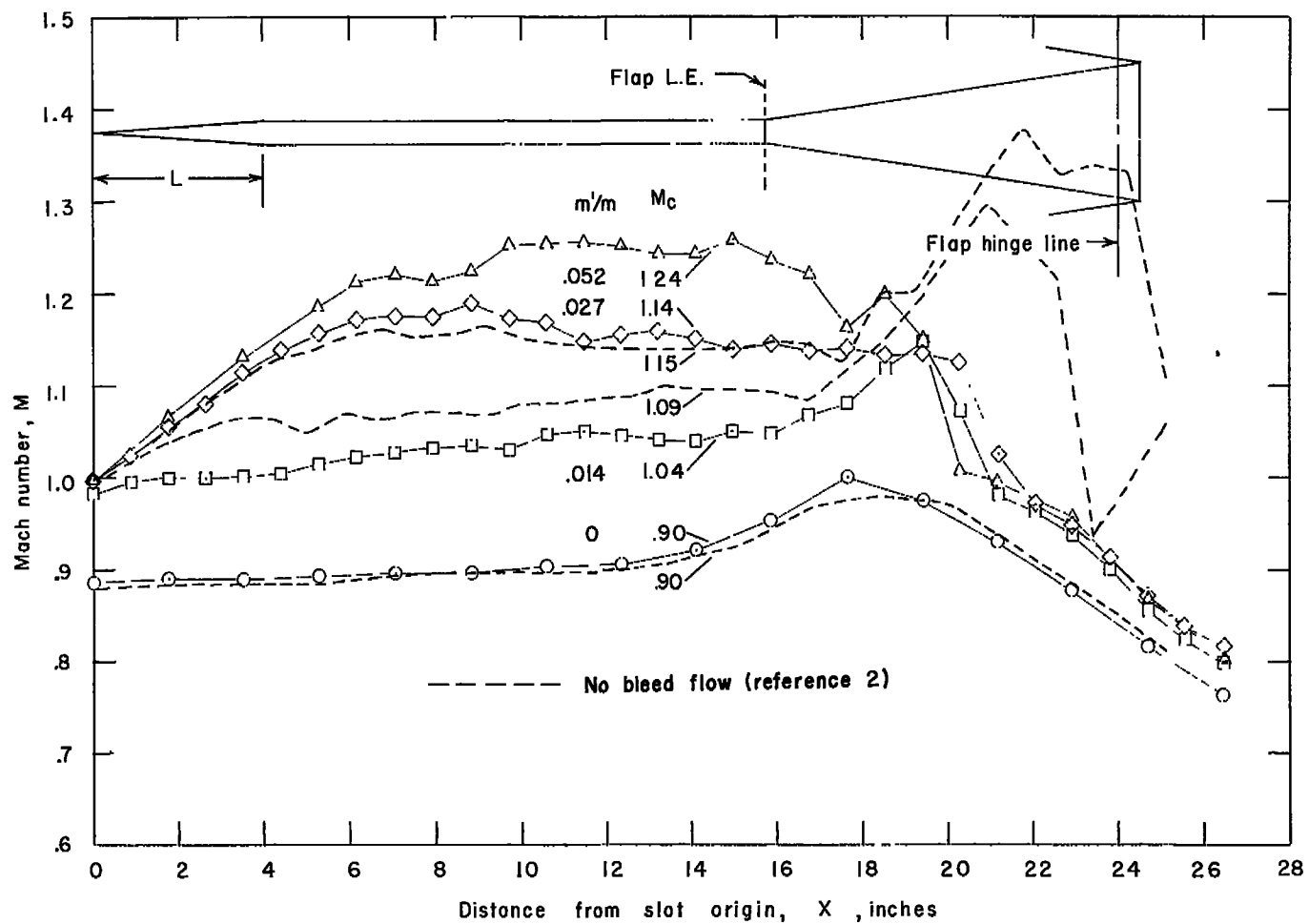
(a) $\frac{H_0}{H_e}$ variable.

Figure 4.- Variation of Mach number M_c with bleed flow.



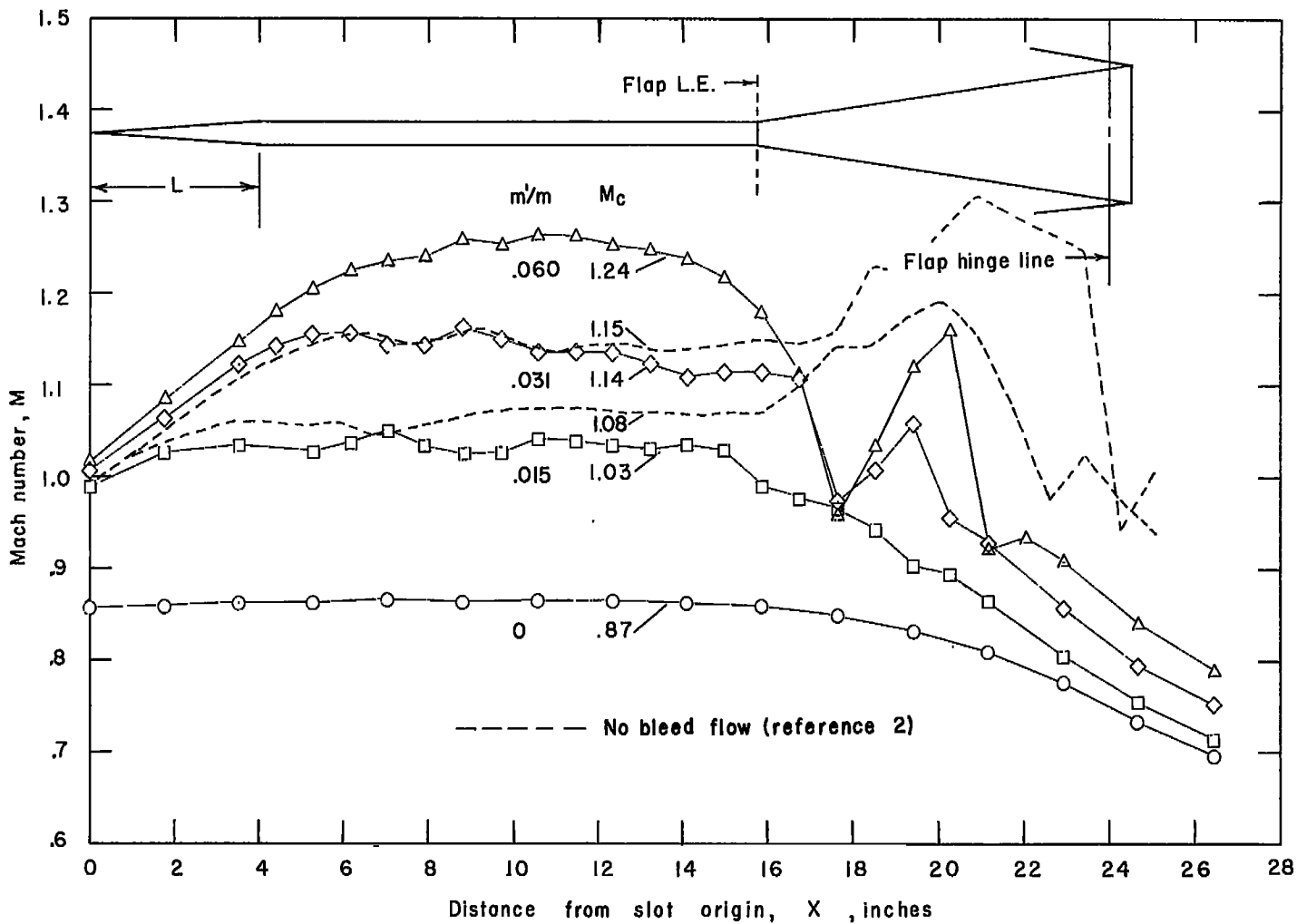
(b) Variation when $\frac{H_o}{H_e}$ is constant.

Figure 4.- Concluded.



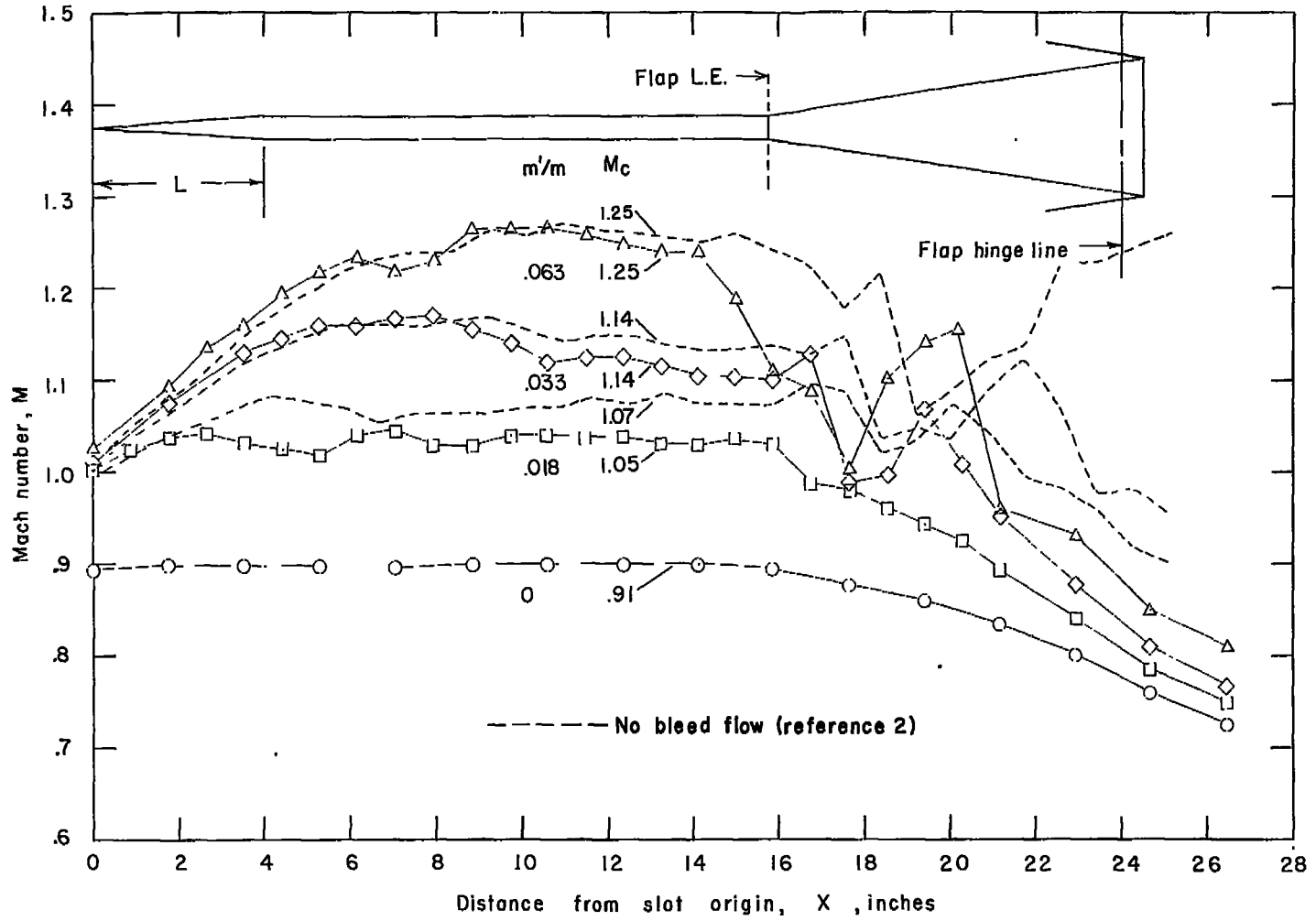
(a) $\delta_f = 0^\circ$.

Figure 5.- Center-line Mach number distributions. $\frac{nw_s}{C/4} = \frac{1}{7}$; $\frac{L}{h} = \frac{1}{2}$; long flap.



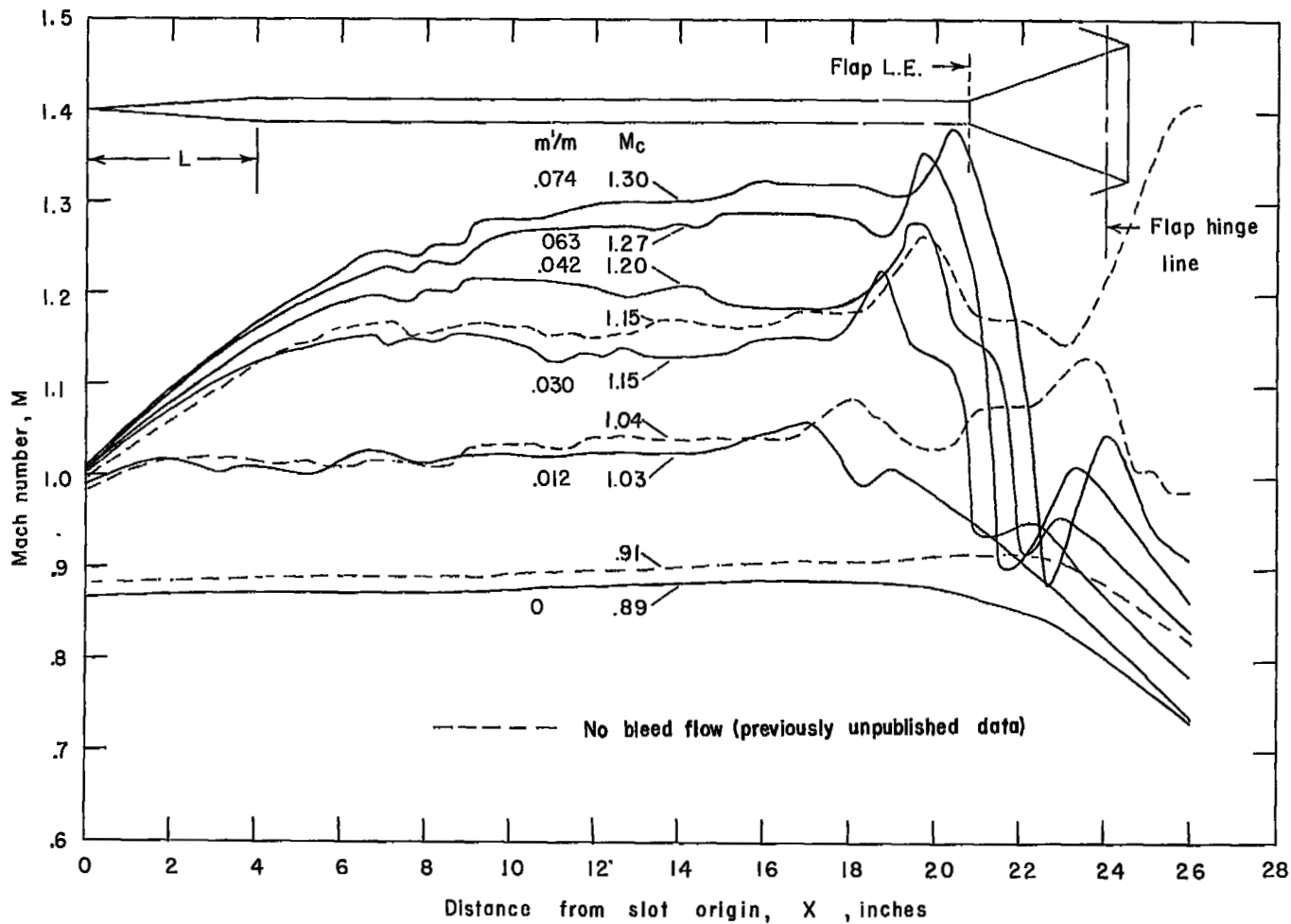
(b) $\delta_f = 5^\circ$.

Figure 5.- Continued.



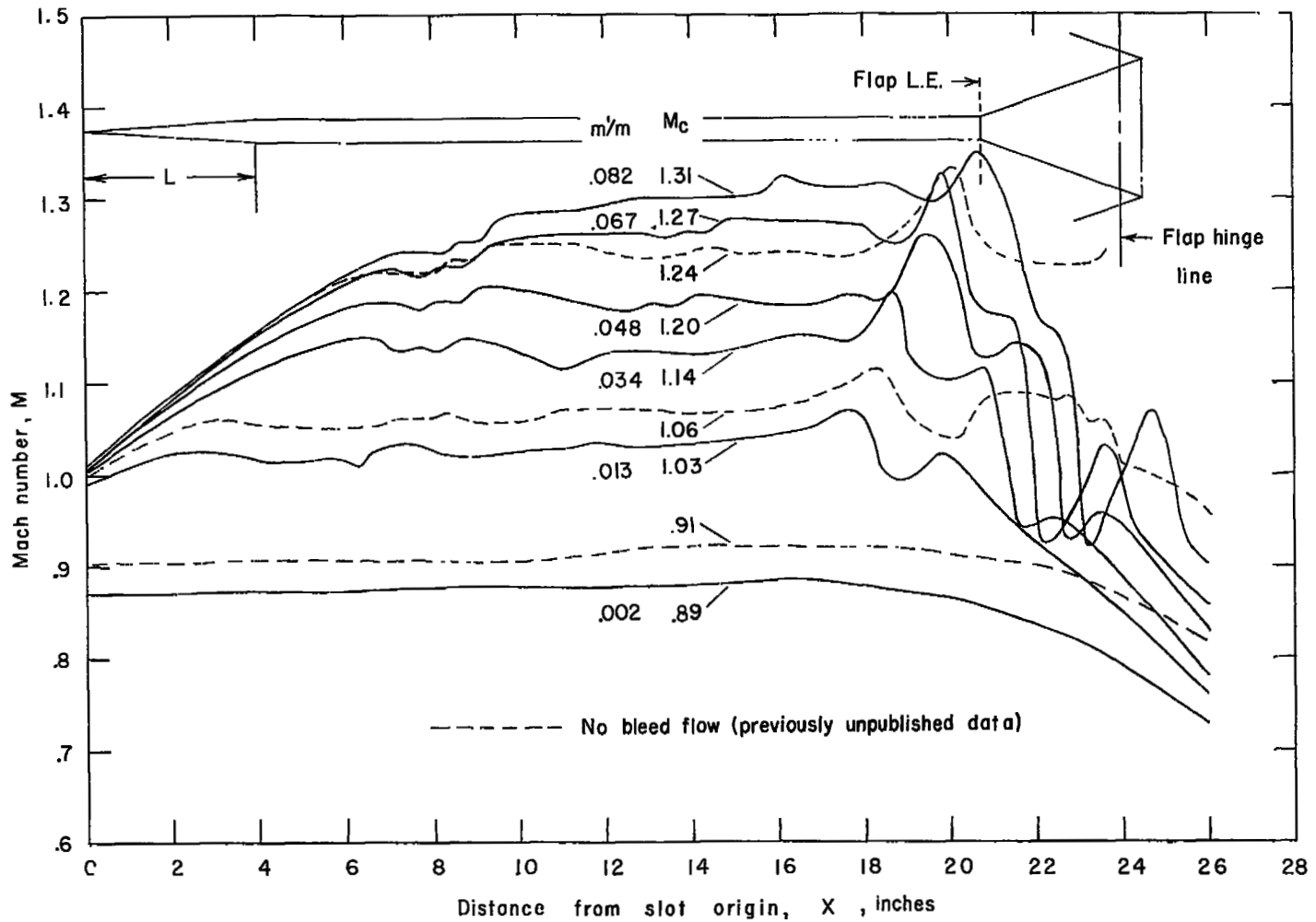
(c) $\delta_f = 10^\circ$.

Figure 5.- Concluded.



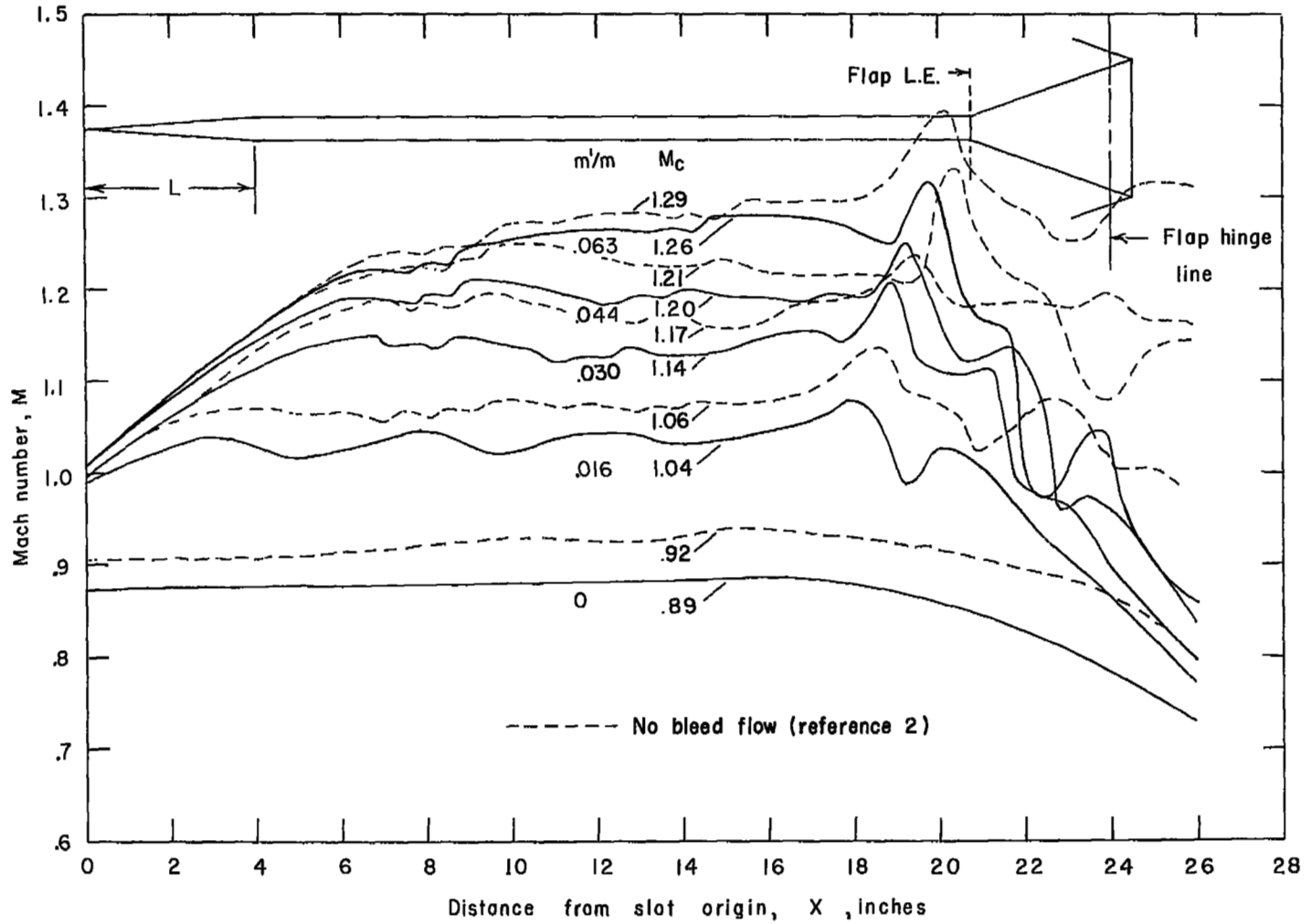
(a) $\delta_f = 0^\circ$.

Figure 6.- Center-line Mach number distributions. $\frac{nw_s}{c/4} = \frac{1}{7}$; $\frac{L}{h} = \frac{1}{2}$; short flap.



(b) $\delta_f = 5^\circ$.

Figure 6.- Continued.



(c) $\delta_f = 10^\circ$.

Figure 6.- Concluded.

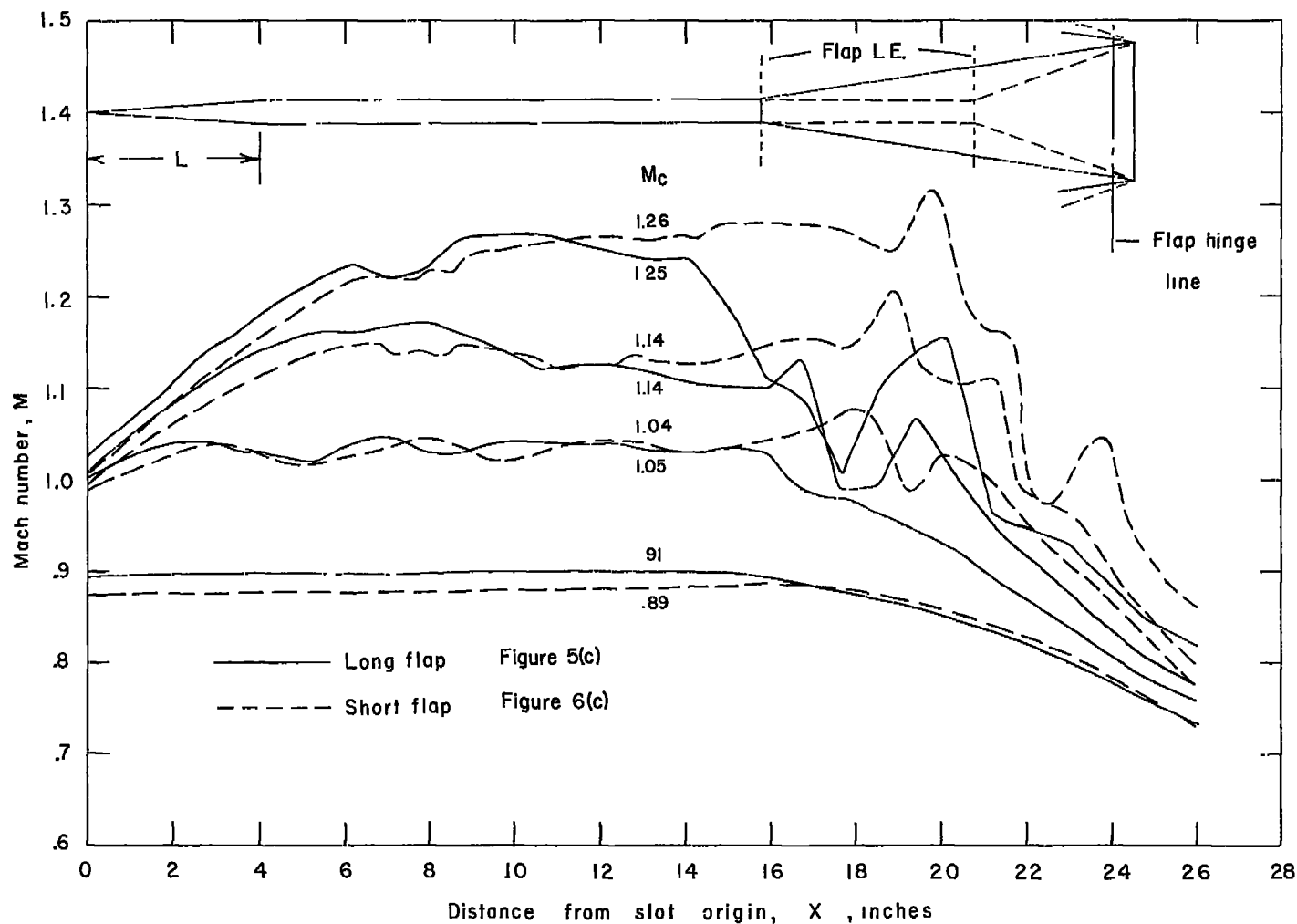


Figure 7.- Comparisons of center-line Mach number distributions. Long and short flaps with bleed flow; $\frac{D_{WS}}{C/4} = \frac{1}{7}$; $\frac{l_f}{h} = \frac{1}{2}$; $\delta_f = 10^\circ$.

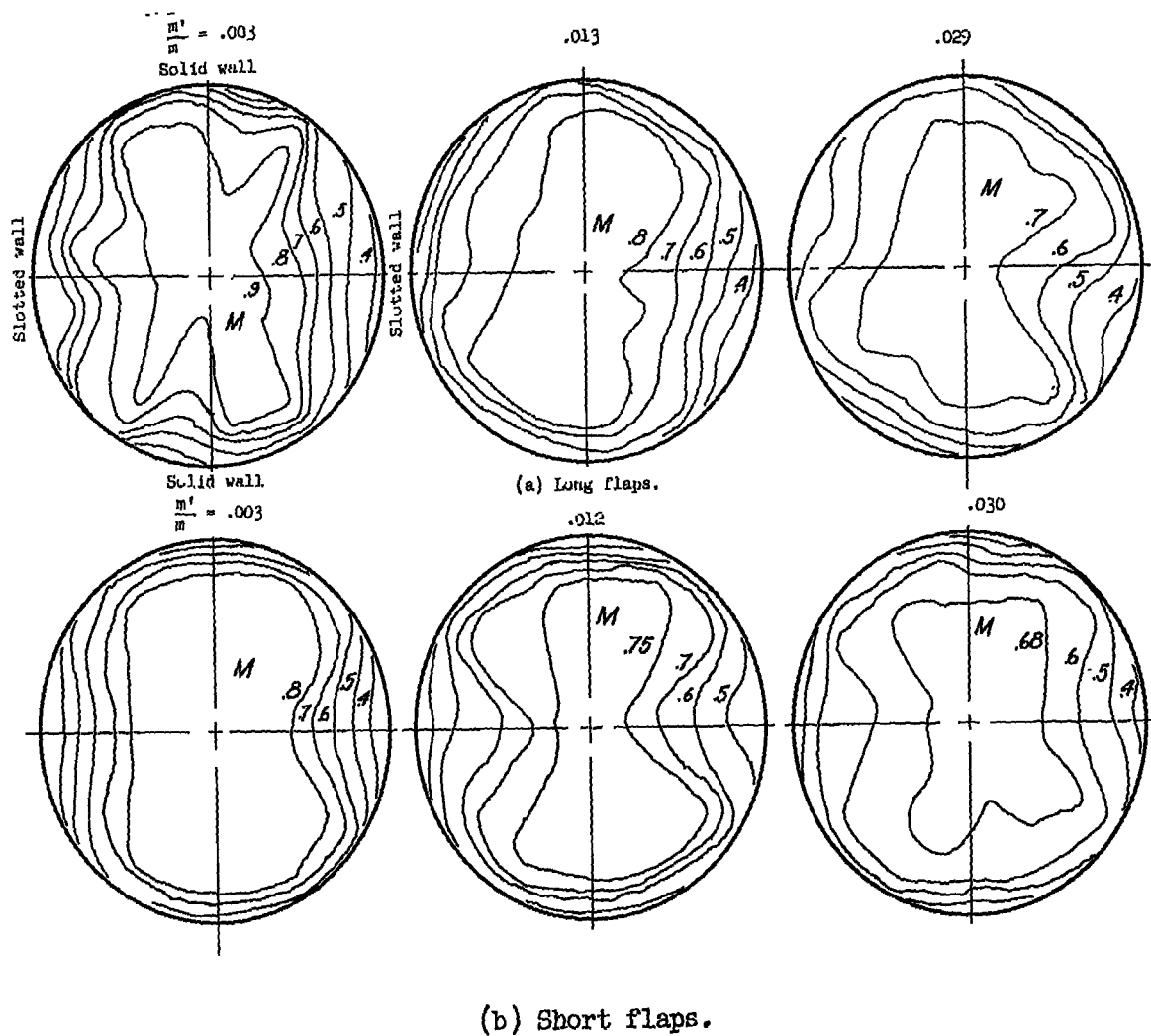


Figure 8.- Diffuser-inlet Mach number contours at $M_c = 1.15$ with varying bleed.

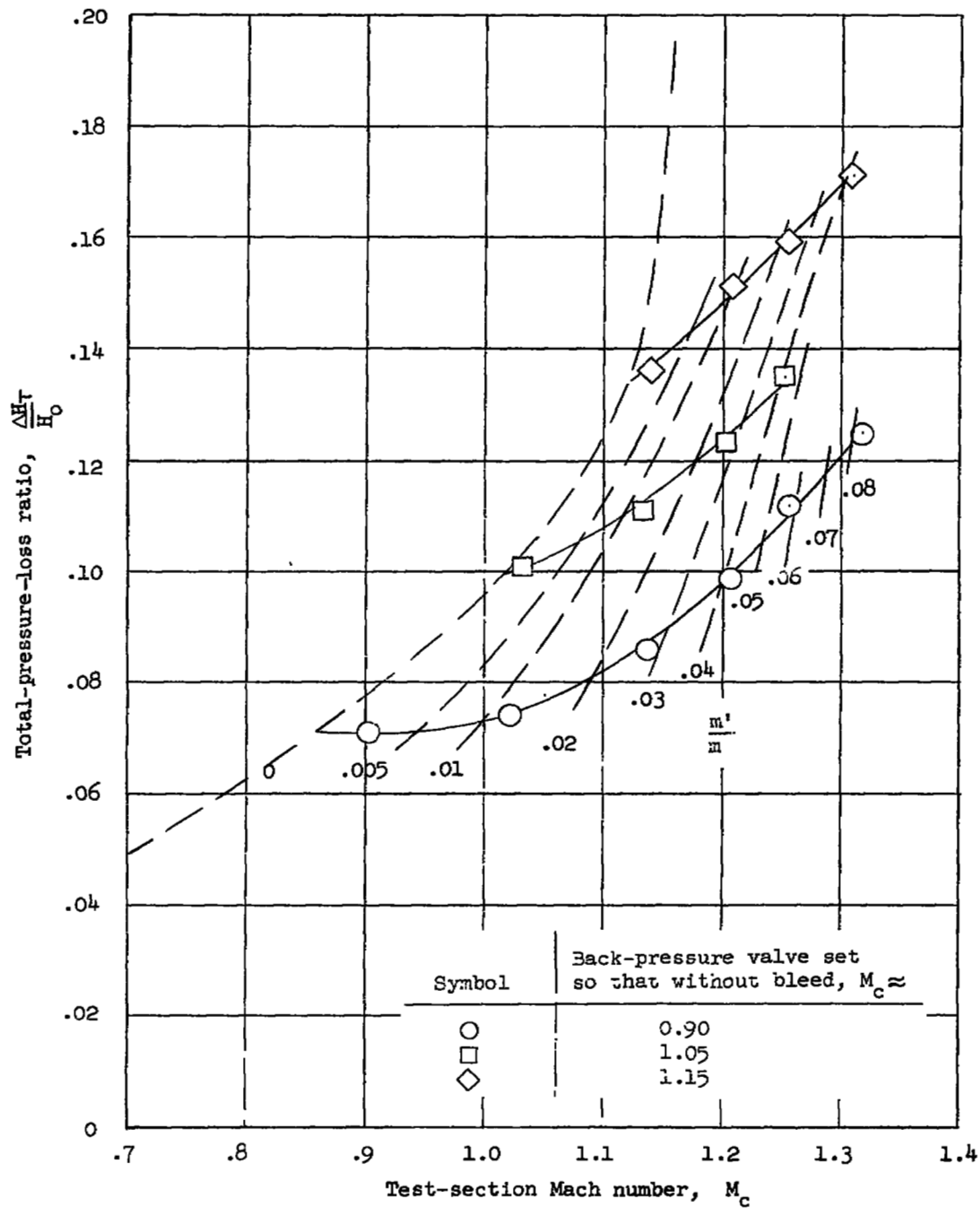
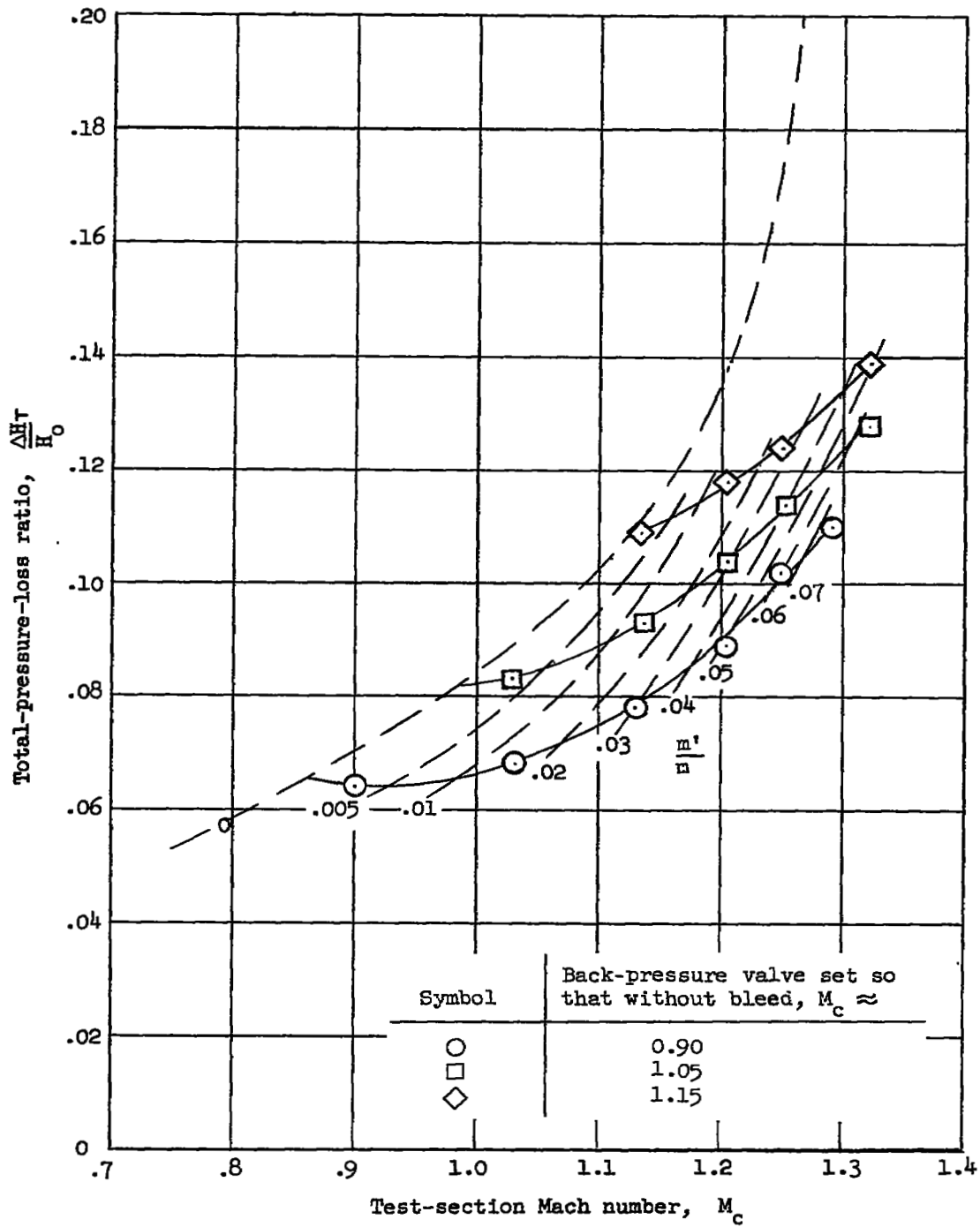
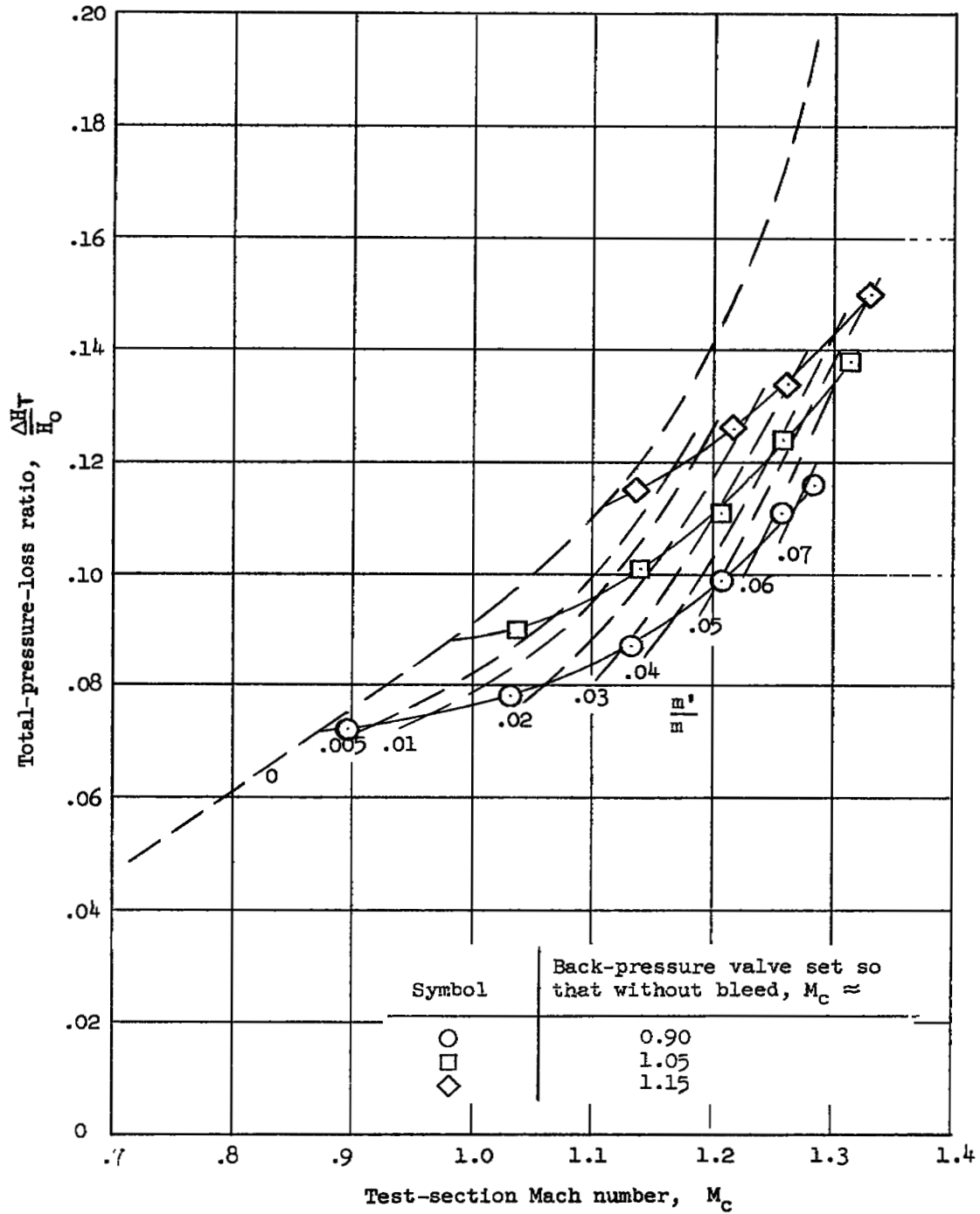
(a) $\delta_F = 0^\circ$.

Figure 9.- Variation of total-pressure loss with test-section Mach number for different bleed flow rates. Long-flap configuration.



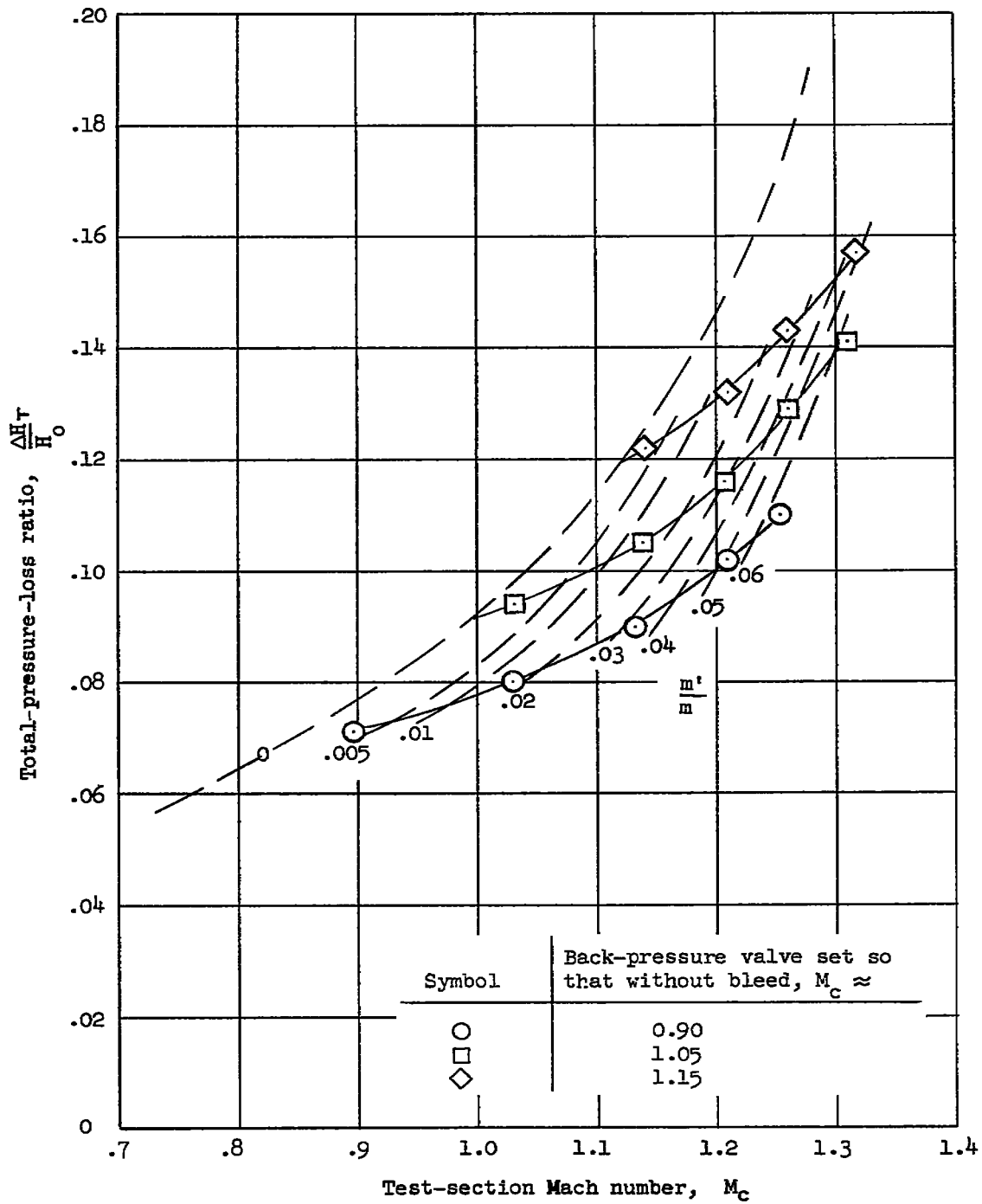
(b) $\delta_F = 5^\circ$.

Figure 9.- Continued.



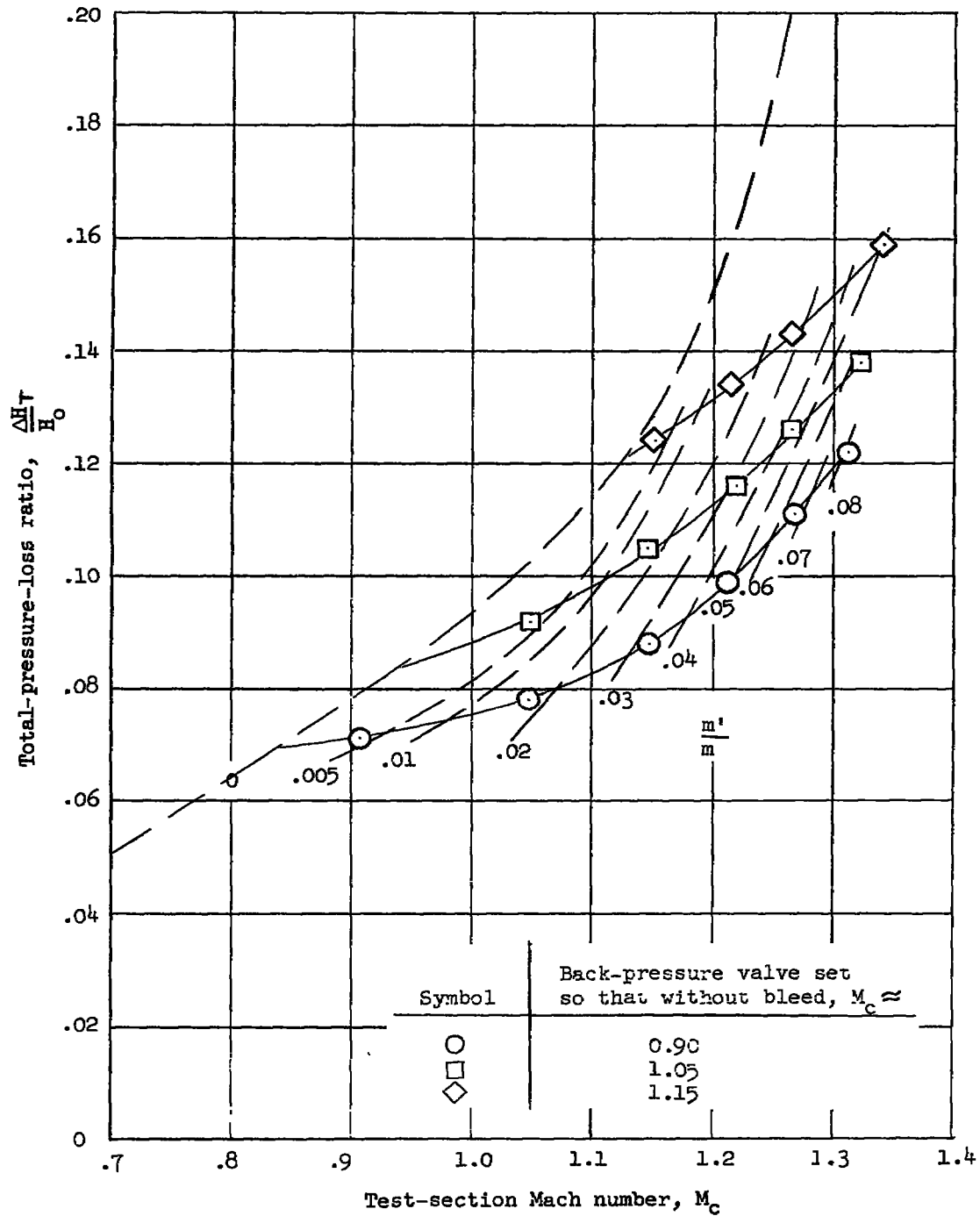
(c) $\delta_F = 10^\circ$.

Figure 9.- Continued.



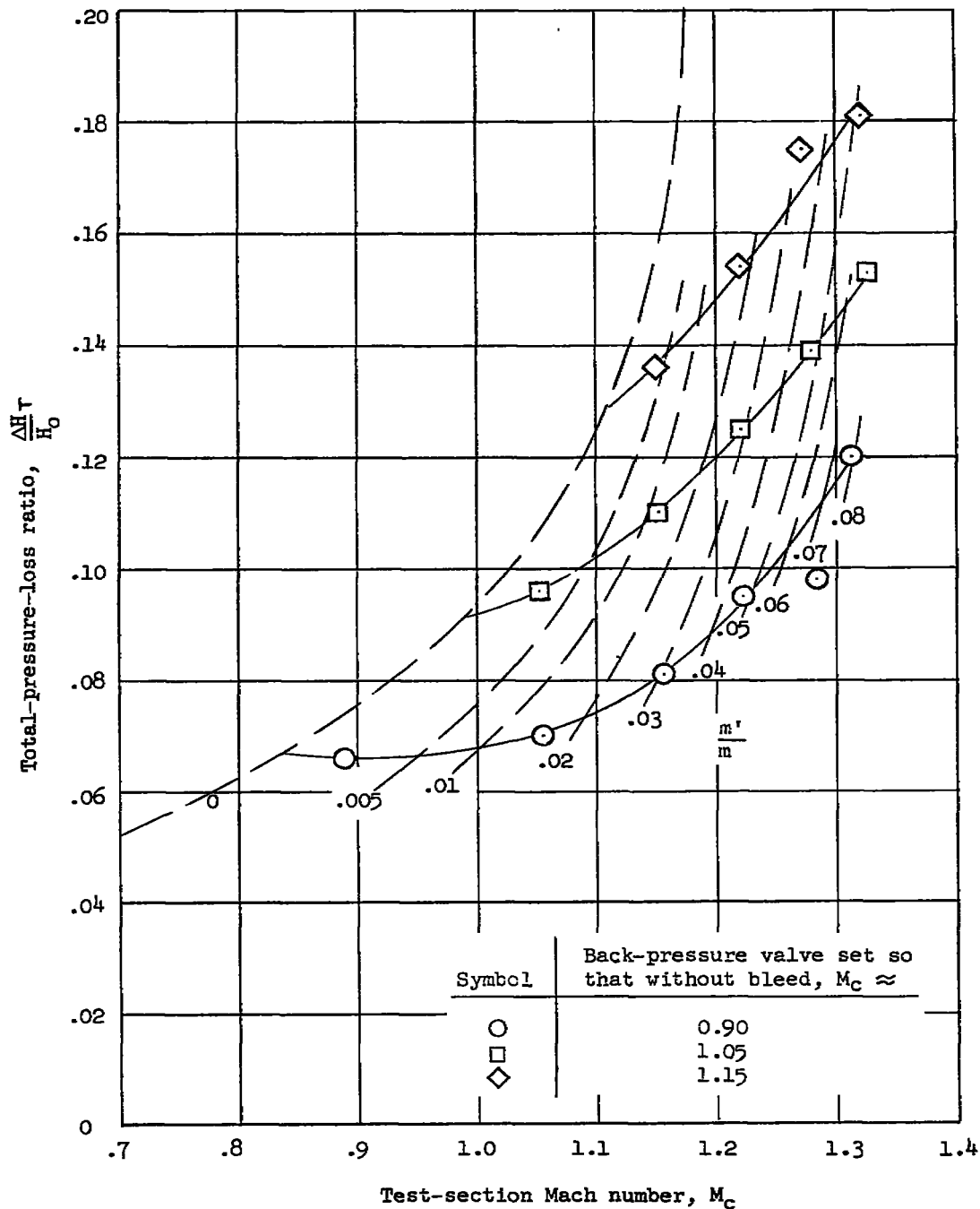
(d) $\delta_F = 15^\circ$.

Figure 9.- Continued.



(e) $\delta_F = 20^\circ$.

Figure 9.- Concluded.



(a) $\delta_F = 0^\circ$.

Figure 10.- Variation of total-pressure loss with test-section Mach number for different bleed flow rates. Short-flap configuration.

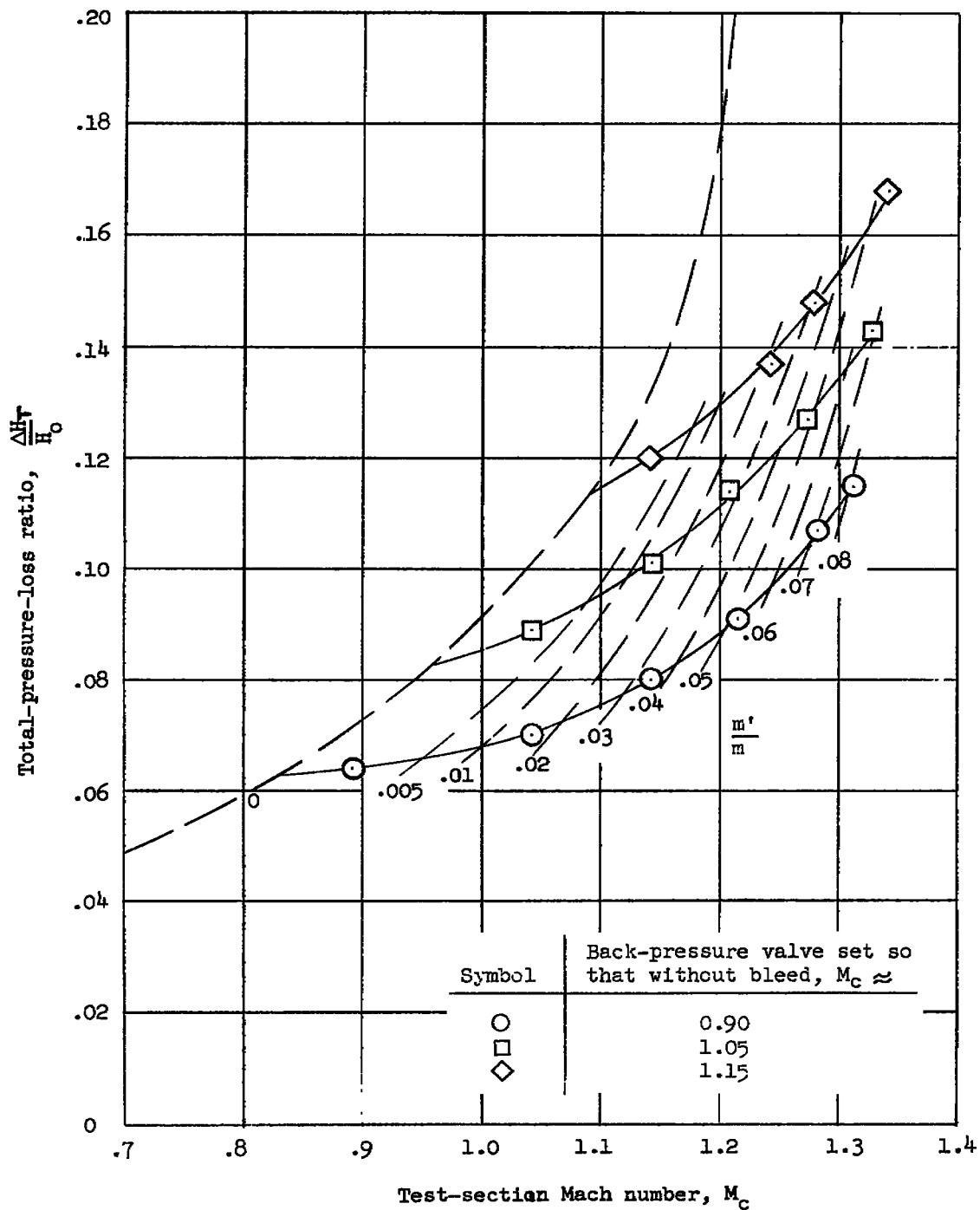
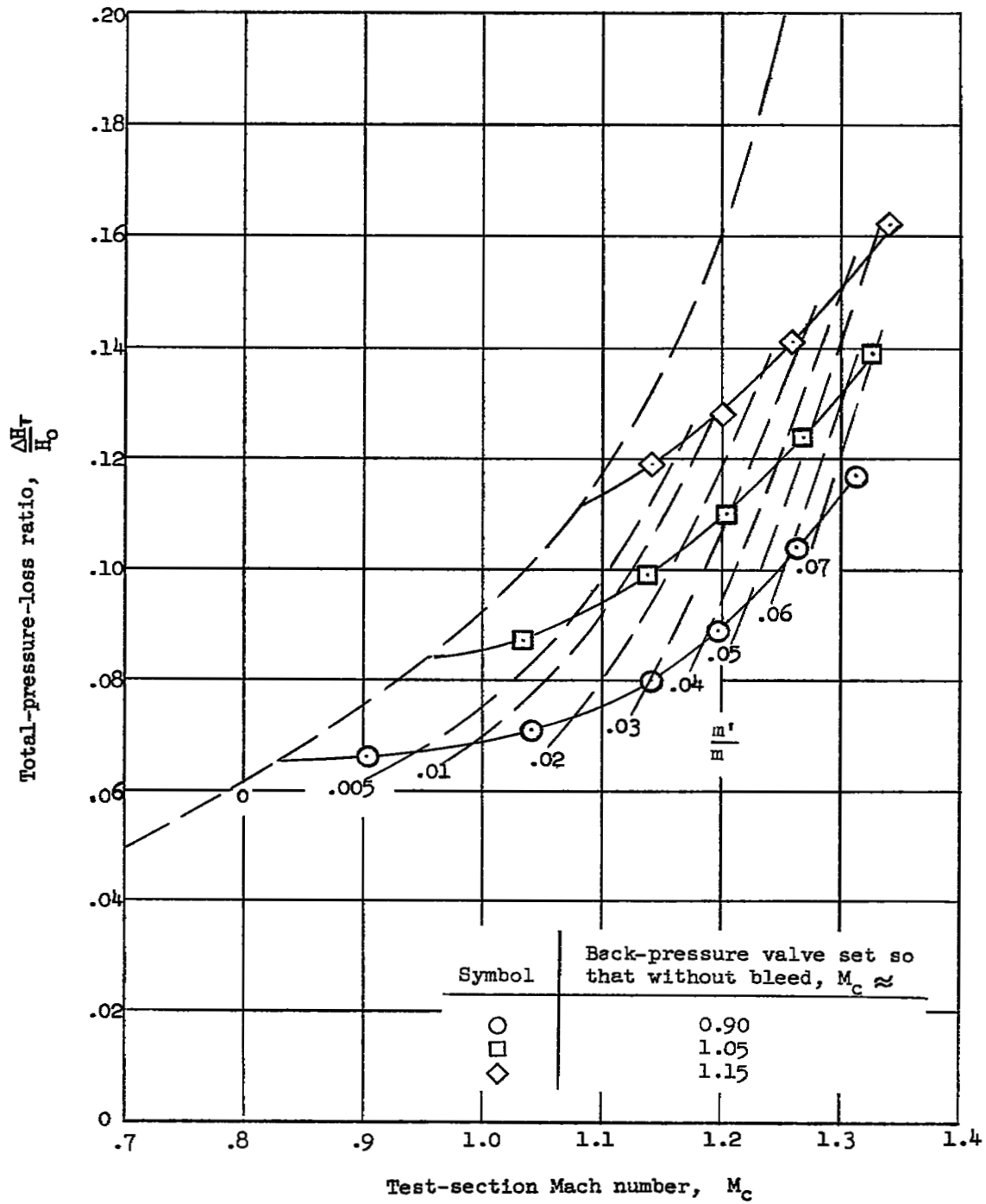
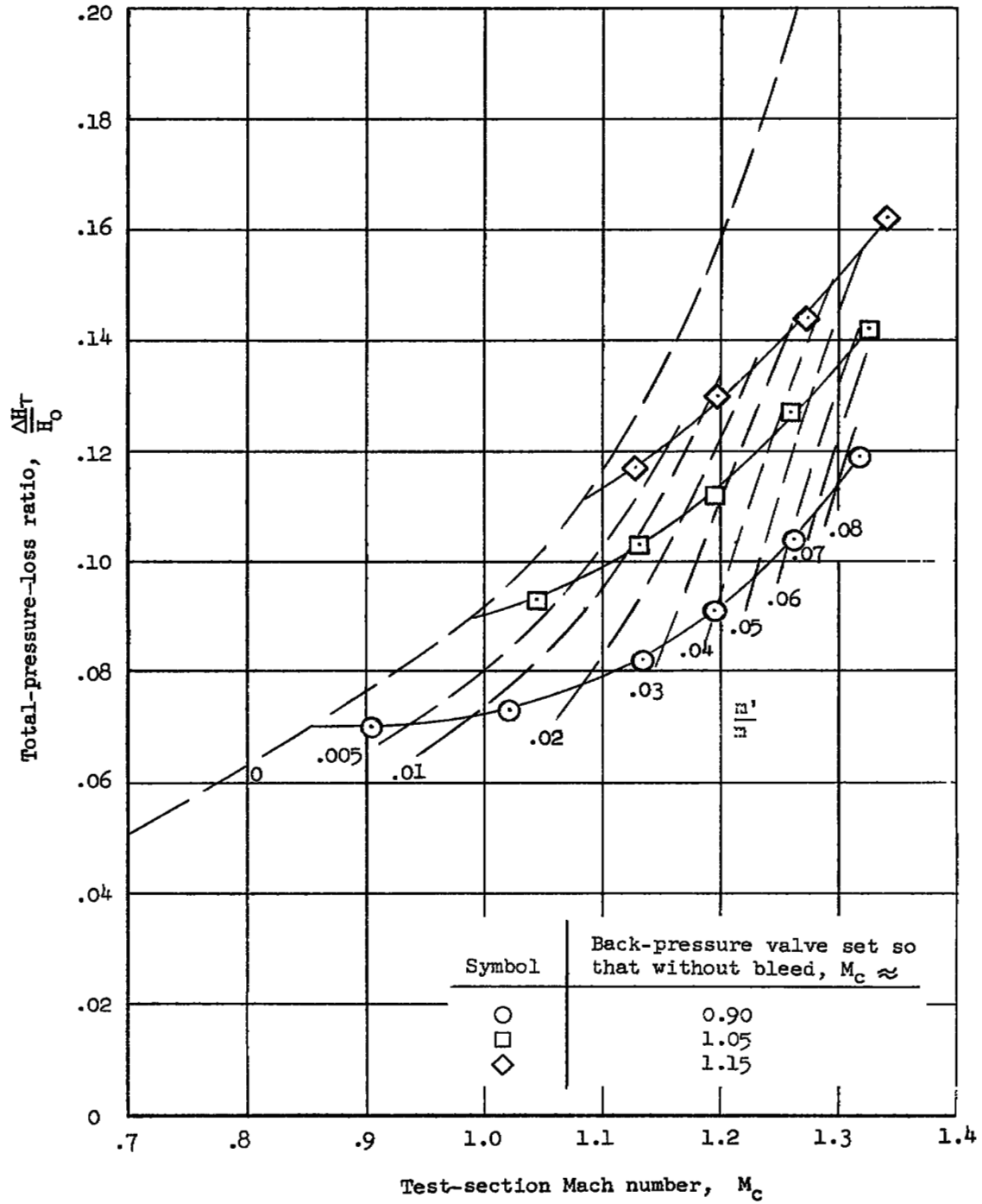
(b) $\delta_F = 5^\circ$.

Figure 10.- Continued.



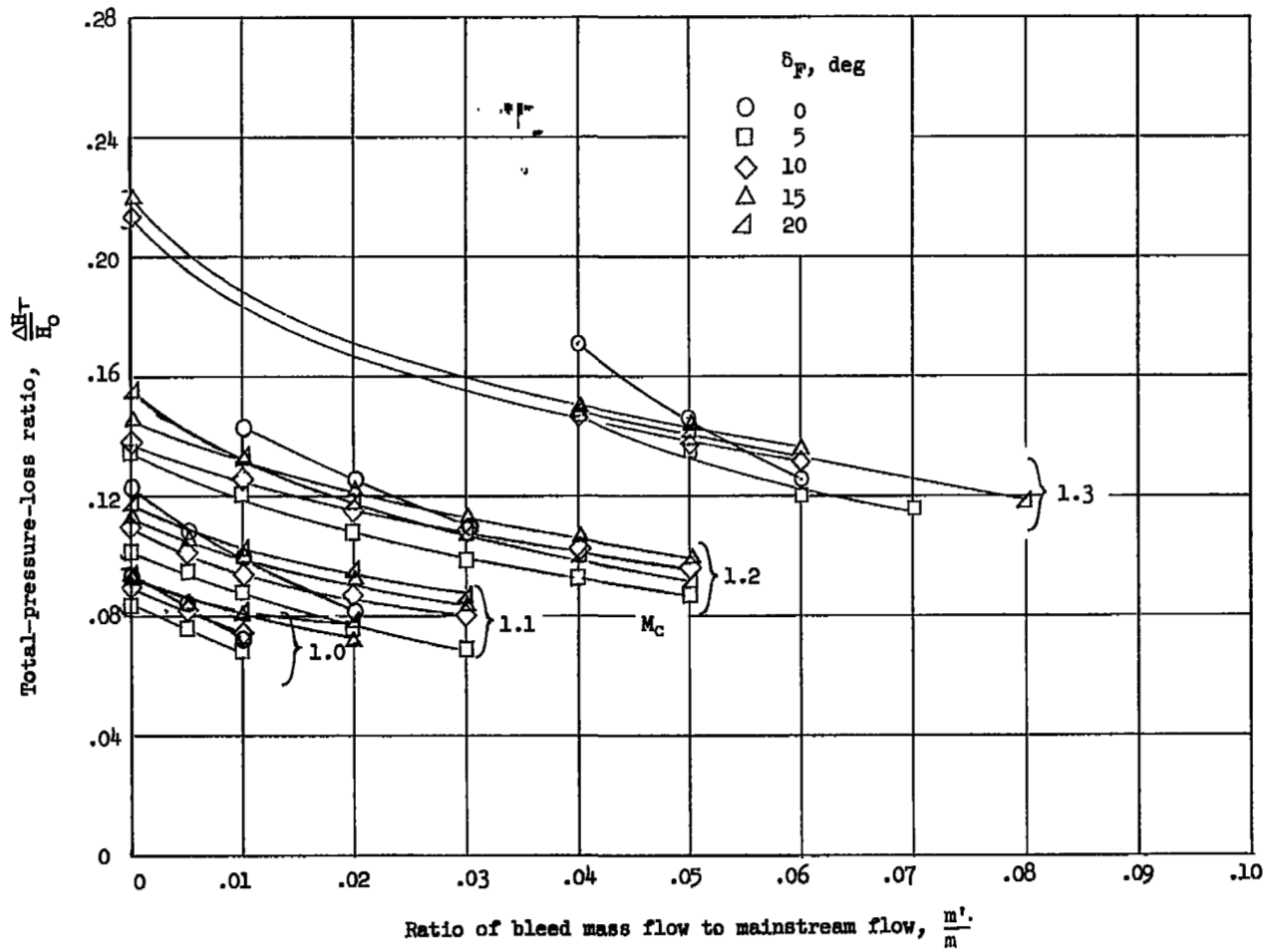
(c) $\delta_F = 10^\circ$.

Figure 10.- Continued.



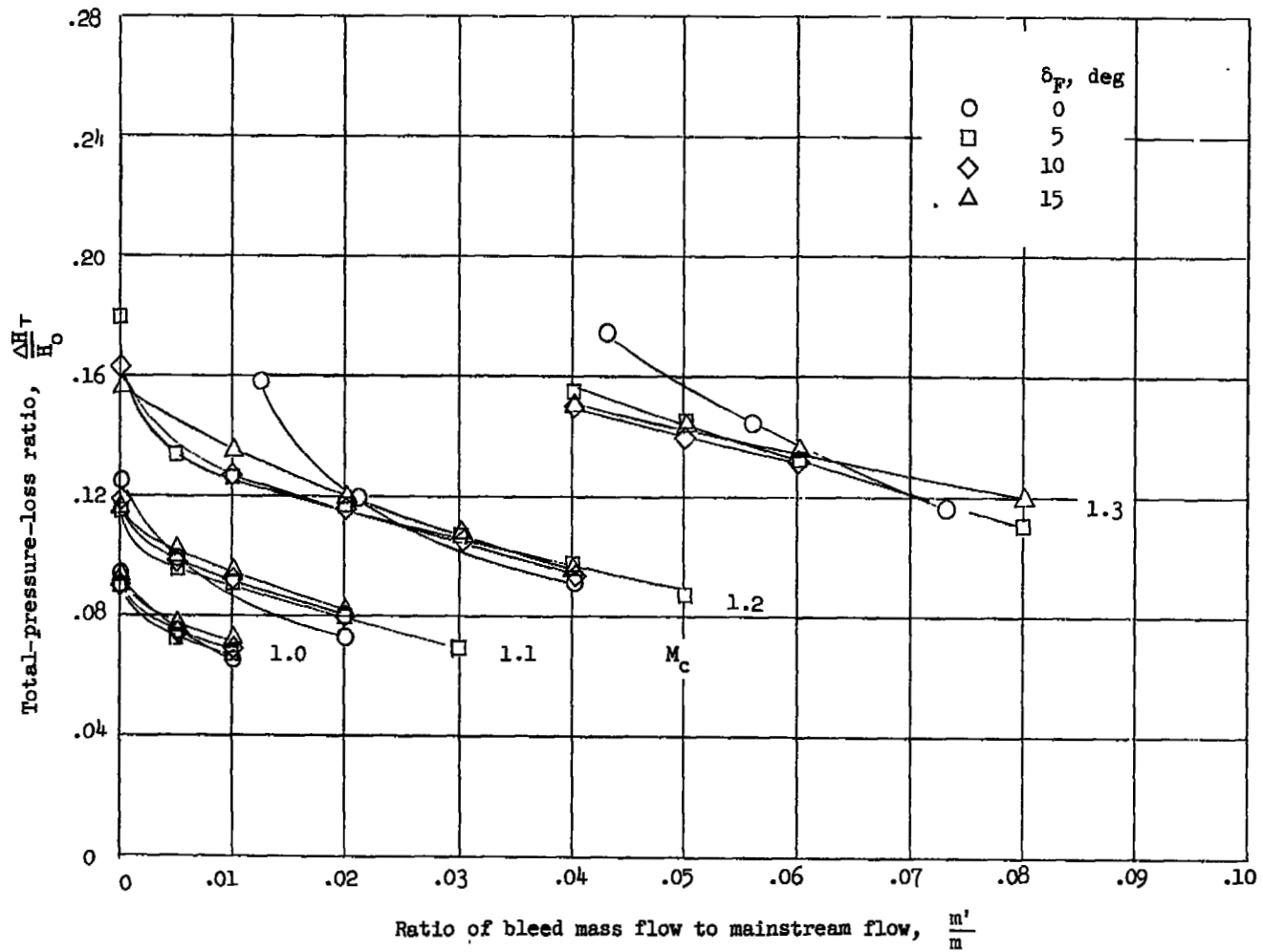
(d) $\delta_F = 15^\circ$.

Figure 10.- Concluded.



(a) Long-flap configuration.

Figure 11.- Variation of total-pressure loss with bleed flow for constant Mach numbers.



(b) Short-flap configuration.

Figure 11.- Concluded.

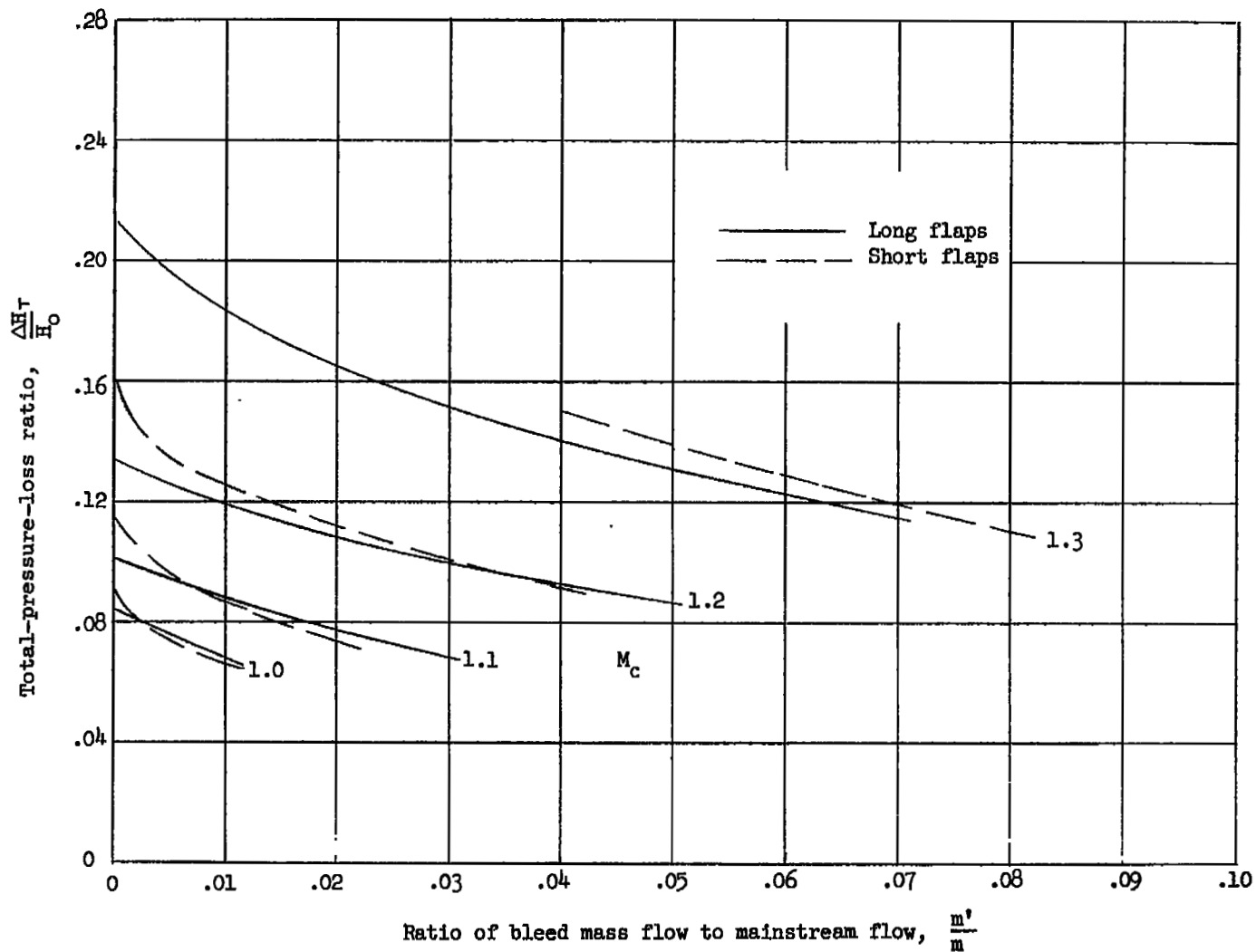
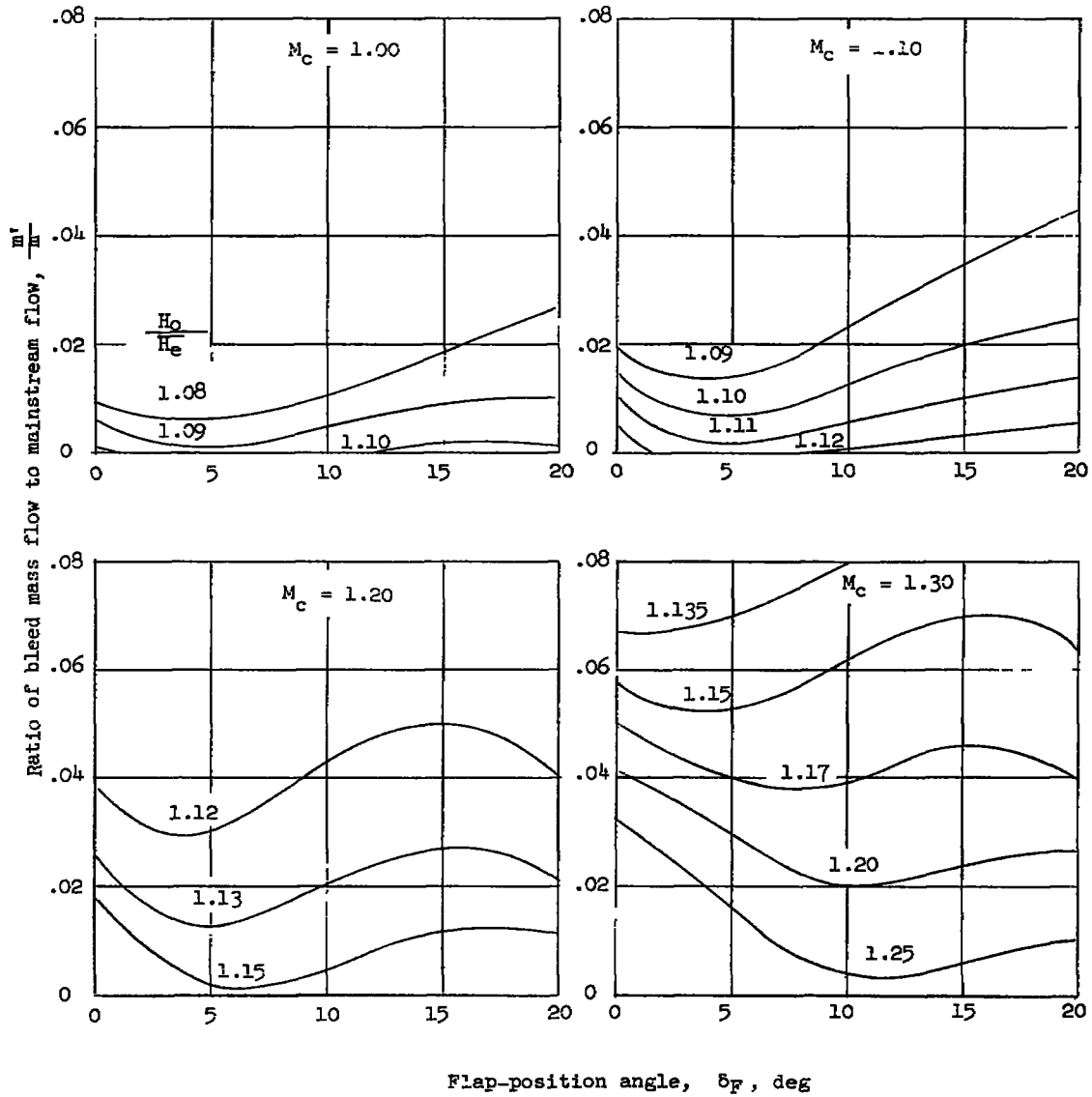
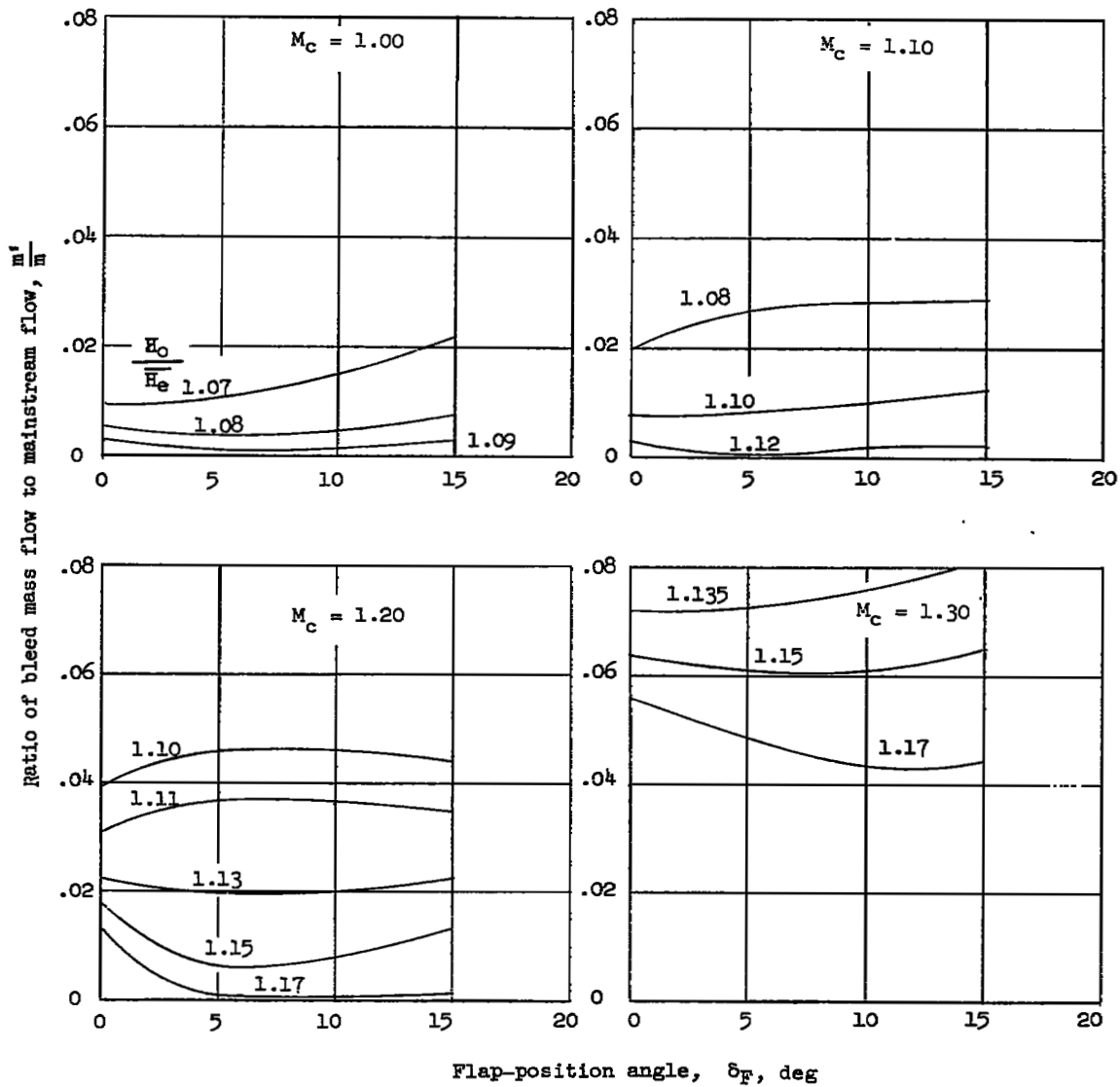


Figure 12.- Envelope curves comparing total-pressure-loss variation with bleed flow for long- and short-flap configurations.



(a) Long-flap configuration.

Figure 13.- Effect of flap setting on bleed flow required.



(b) Short-flap configuration.

Figure 13.- Concluded.

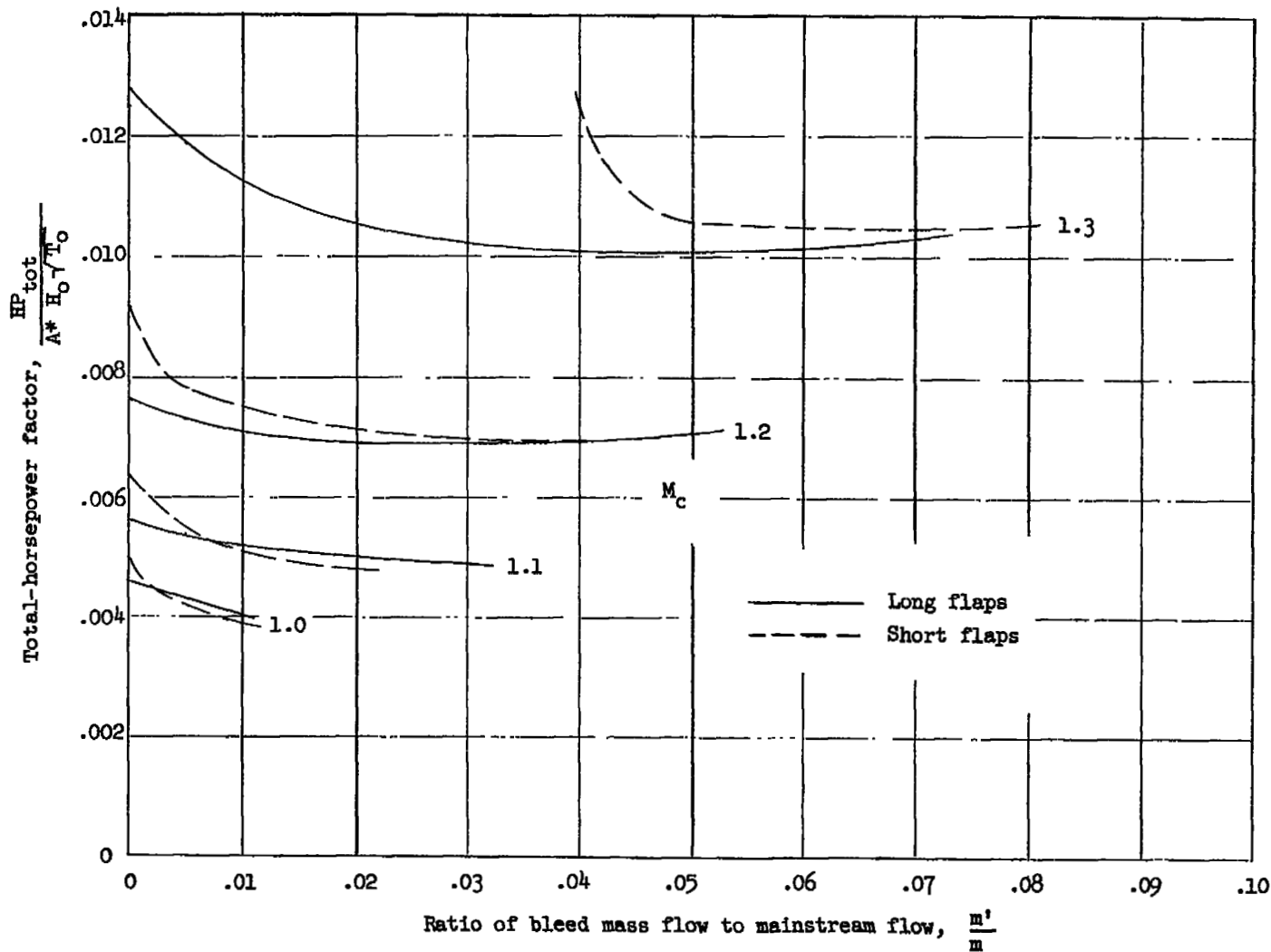


Figure 14.- Envelope curves comparing total-horsepower-factor variation with bleed flow for long- and short-flap configurations.

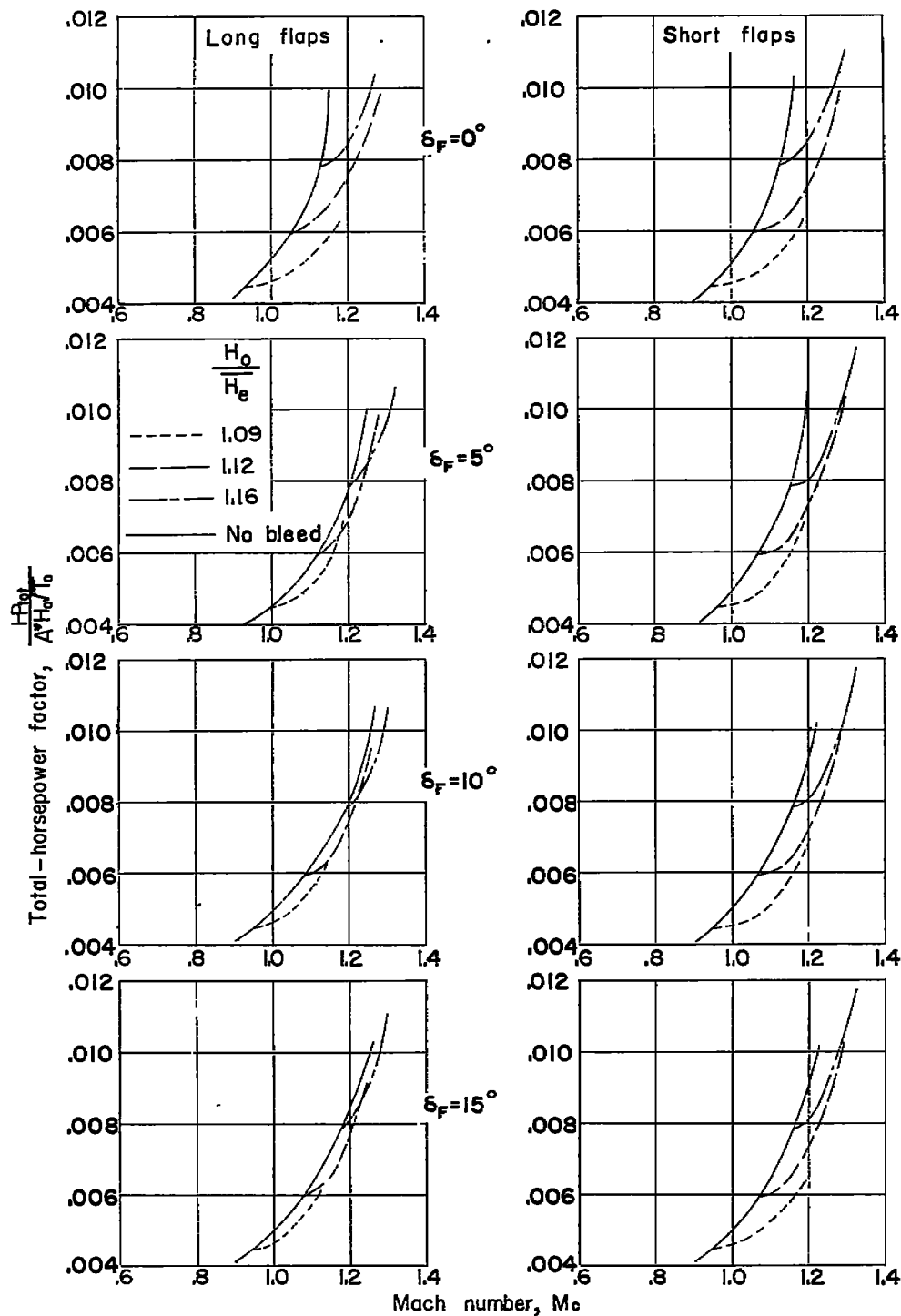


Figure 15.- The effects of Mach number on total horsepower with bleed flow initiating at different Mach numbers.

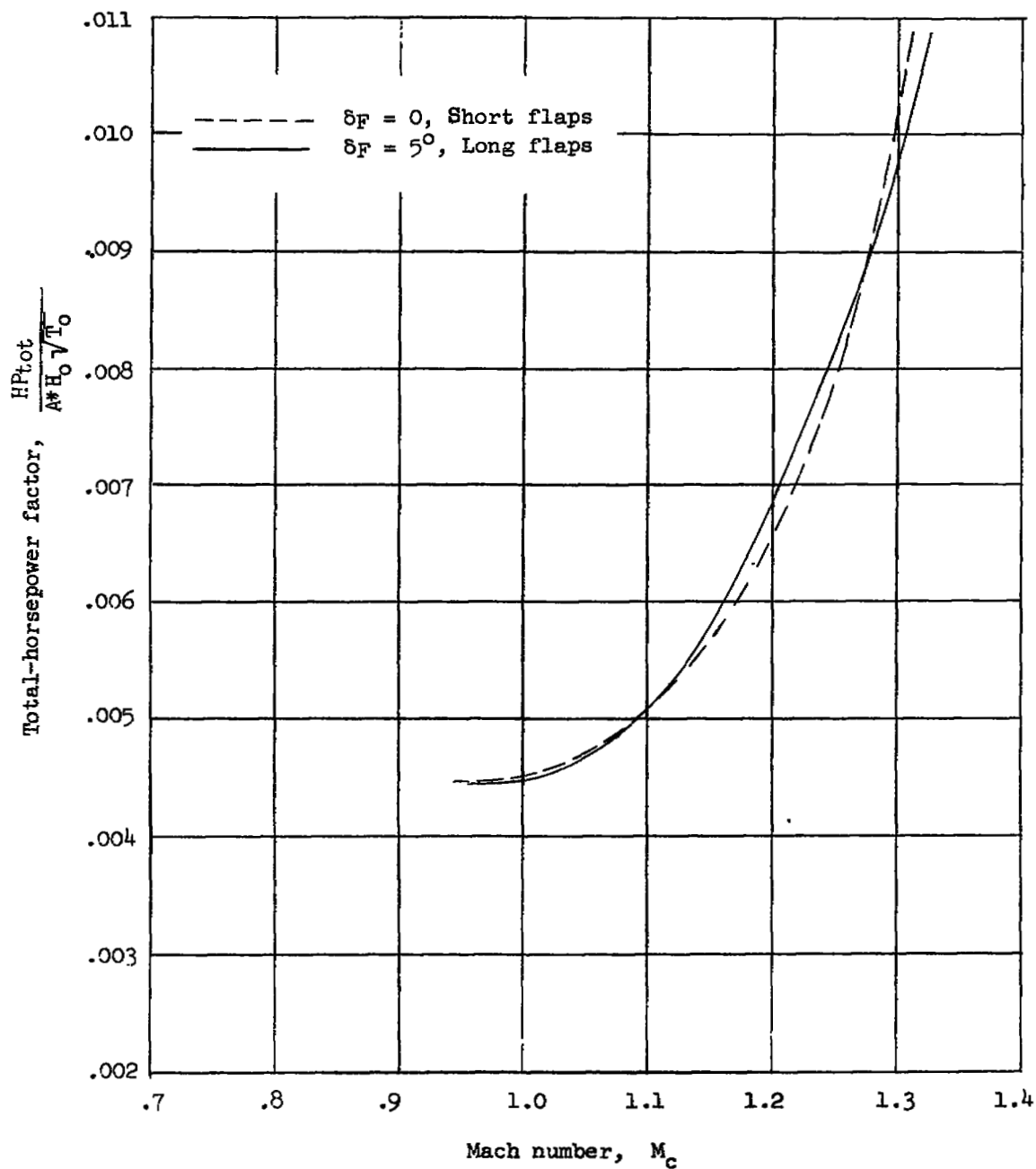


Figure 16.- Total horsepower for best performance conditions. Long- and short-flap configurations.

NASA Technical Library



3 1176 01437 6744

